DETERMINING SURFACE AND GROUNDWATER INTERACTION FOR AN ENTRENCHED COASTAL STREAM BASED ON STREAMBED TEMPERATURE TIME-SERIES ANALYSIS UTILIZING SEVERAL TECHNIQUES

A Thesis

by

CHESTER G. SCOTCH

AS, Del Mar College, 2009
BS, Texas A&M University-Corpus Christi, 2011

Submitted in Partial Fulfillment of the Requirements for the Degree of

MASTER OF SCIENCE

in

ENVIRONMENTAL SCIENCE

Texas A&M University-Corpus Christi
Corpus Christi, Texas

December 2016

December 2016

DETERMINING SURFACE AND GROUNDWATER INTERACTION FOR AN ENTRENCHED COASTAL STREAM BASED ON STREAMBED TEMPERATURE TIME-SERIES ANALYSIS UTILIZING SEVERAL TECHNIQUES

A Thesis

by

CHESTER G. SCOTCH

This thesis meets the standards for scope and quality of
Texas A&M University-Corpus Christi and is hereby approved.

Dorina Murgulet, PhD
Chair

James Constantz, PhD
Committee Member

Paul Montagna, PhD
Committee Member

December 2016

ABSTRACT

Surface water exchange with groundwater has become an increasingly active area of investigation since the 1980's, as researchers have recognized them as a hydrologic continuum. Wide ranges of hydrologic setting have been investigated, though very few studies have investigated these exchanges in coastal streams in semi-arid environments. This study's objective is to improve the understanding of groundwater-surface water interaction in a coastal low-flow streambed, characterized by relatively high clay contents, by implementing a combination of analytical, mathematical, statistical, and geophysical methods.

Thermal responses resulting from heat transfer due to conduction (no groundwater movement) and advection (by groundwater transport) are analyzed in a streambed characterized by low hydraulic gradients and conductivity sediments with possibly diffusive and small-scale flow paths. These characteristics provide a challenge when attempting to quantify surface and groundwater fluxes utilizing traditional methods. A new approach to separate heat advection from conduction through decomposition of temperature time-series data is proposed.

The estimates provided by the numerical and analytical solutions are consistent and indicate that groundwater upwelling is occurring in the streambed during the summer and winter periods at an average of 9 mm d-1 and 3.5 mm d-1, respectively. However, there were discrepancies in specific discharge with depth, indicating multi-dimensional flow in the hyporheic zone. The decomposition method results suggest it may not be applicable

to fine-textured coastal stream sediments. Resistivity results provided a good first order approximation of groundwater discharge and serves as a reliable validation tool for thermal methods. The overall results of this study confirm that thermal methods are capable of quantifying surface and groundwater interaction in a coastal low-flow stream.

Because coastal streams flow into environmentally and economically sensitive bays and estuaries that serve as key ecosystems and breeding grounds for a large variety of species along coastal areas, improving scientific understanding of groundwater discharge is of significance since it can serve as a transport mechanism for contaminants into these environments. Further research should be conducted to quantify multi-dimensional flows in the hyporheic zone.

ACKNOWLEDGEMENTS

Writing this thesis took considerable effort and most certainly could not have been accomplished without the support and assistance of many folks. I would like to thank all of those who spent long-hot hours in the South Texas heat assisting in data collection. I would like to thank Rick Hay for his help with data processing and for ensuring there was always hot coffee at the ready. I also want to extend my appreciation to all members of my committee; Dr. James Constantz, Dr. Paul Montagna and Dr. Dorina Murgulet. Special thanks go out to my advisor, Dr. Dorina Murgulet, who inspired me to accept this daunting task and Dr. James Constantz for elucidating the fundamental principles.

TABLE OF CONTENTS

CONTENTS PAGE

ABSTRACT v

ACKNOWLEDGEMENTS vii

TABLE OF CONTENTS viii

LIST OF FIGURES x

LIST OF TABLES xi

1. Introduction 1

1.1. Use of Tracers and Analytical and Numerical Techniques 1

1.2. Unique Hydrology and Ecology of Texas Coastal Low-Flow Streams. 6

1.3. Research Objectives. 7

2. Data and Methods. 8

2.1. Study Site 8

2.2. Data Acquisition 9

2.3. Raw Data Pre-processing with R 12

2.4. Data Analysis 14

2.4.1. Analytical Method: Type Curves 14

2.4.2 Numerical Method: VS2DH 22

2.4.3. Statistical Method: Seasonal-trend decomposition (STL) 25

2.4.4 Geophysical Method: Electrical Resistivity 27

3. Results and Discussion 32

3.1. Analytical Method: Type Curves 32

3.2. Numerical Method Results and Discussion: VS2DH/1DTempPro 35

3.3. Statistical Method: STL 41

3.4. Geophysical Method: Electrical Resistivity 49

4. Conclusions 55

5. Summary 58

Literature Cited 58

Appendices: 66

LIST OF FIGURES

FIGURES PAGE

Figure 1: Map of Study Site....9

Figure 2: Profiler Diagram....10

Figure 3: Type Curve....14

Figure 4: Analytical Method Diagram....20

Figure 5: Summer and Winter Period Thermograph....21

Figure 6: Summer 33 cm Modeled vs Observed....39

Figure 7: Winter 33 cm Modeled vs Observed....40

Figure 8: Summer 66 cm Modeled vs Observed....40

Figure 9: Winter 66 cm Modeled vs Observed....41

Figure 10: SB08 Decomposition....42

Figure 11: Generation of the Random Component....43

Figure 12: Summer Random Components....45

Figure 13: Winter Random Components....45

Figure 14: ERT Tomographs....52

Figure 15: Stream Location and Box Zone....54

LIST OF TABLES

TABLES PAGE

Table 1: Analytical Method Estimated Specific Discharges 33

Table 2: Parameters Used in VS2DH Modeling.....36

Table 3: 1DTempPro Model Results 37

Table 4: Decomposition Derived Specific Discharge.....46

Table 5: TBR Derived Resistivities 50

Table 6: ERT Derived Specific Discharge.....53

Table 7: Summary of Results from the Different Methods 56

1. Introduction

Although surface water (i.e. streams, lakes, estuaries) and groundwater are often referred to as separate hydrologic systems, they are intimately related as a change in one can ultimately affect the other [*Constantz and Stonestrom*, 2003]. Since these two entities act as linked pathways for contaminant transport in the hydrologic cycle, a comprehensive understanding of the groundwater-surface water relationship is essential for improved water resource management practices. Exchanges occur whenever a hydraulic gradient exists between the two components; a positive gradient, when the water table elevation is higher than that of surface water, results in a gaining stream, while a negative one, when the water table elevation is lower than that of surface water, favors groundwater recharge through a losing stream [*Constantz and Stonestrom*, 2003]. Examination of differences in water elevations between the two hydrologic domains yields information on the direction of flow. However this method may not be practical in some environments with low topographic relief and low conductivity sediments that can result in low-rate, small-scale surface and groundwater exchanges [*Freeze and Cherry*, 1979].

1.1. Use of Tracers and Analytical and Numerical Techniques

Environmental tracers, natural or man-made compounds or isotopes,, among others, are widely used to characterize water movement and transport mechanisms, recharge zones, and quantify groundwater-surface water exchange. Ionic species such as chloride and

bromide, which may occur in water as the result of anthropogenic or natural processes, are commonly used tracers and sometimes. Tracing background concentrations of these constituents as well as injection in high concentrations enables the delineation of surface and groundwater interaction [*Nishikawa et al*., 1999; *Constantz et al*., 2003; Cox et al., 2007]. Stable isotopes of water (i.e. deuterium and oxygen) are also used but their utility is limited due to cost and extensive lab analysis while the use of radiogenic isotopes such as tritium is often met with opposition due to its inherent hazards [*Davis*, 1980]. However, Constantz et al. [2003] and Cox et al.[2007] showed that some natural and injected tracers are well suited for exploring surface and groundwater interactions especially when combined with other types of tracers such as natural heat.

While some of the aforementioned are good examples of tracers suitable for surface and groundwater interaction analysis, the use of injected chemicals is often limited spatially and temporally and is frequently constrained by other factors. These tracers are usually restricted to small areas and in most cases are only traceable for a short time after injection. Factors affecting tracer performance include reactivity with and adsorption to the medium through which they flow, pre-existing background concentrations that mask the injected concentration, and public concerns regarding the injection of chemicals into the environment, to name a few of the more prominent issues [*Davis*, 1980; *Constantz and Stonestrom*, 2003].

Because water carries measurable amounts of heat, analysis of temperature changes or heat fluxes can be used as a proxy for surface and groundwater interaction. Heat has many advantages over injected or other naturally-occurring tracers. For instance, as a naturally-occurring tracer, heat is free from many of the concerns related to introducing chemical and/or harmful constituents into the environment. Substantial daily and seasonal temperature fluctuations impart distinct thermal profiles that enable intuitive assessments for exploring groundwater-surface water interactions [*Constantz,* 2008]. In addition, temperature is an instantaneous and easily measurable parameter that does not require extensive filed labor and computer processing, thus greatly reducing costs and increasing time-efficiency [*Constantz,* 2008]. Analyses of temperature variation may be well suited for areas with low water exchange rates and numerous small-scale flow paths as indicated by Constantz and Stonestrom [2003]. The basis behind the use of heat as a tracer for surface and groundwater interaction analysis is based on the concept of conduction and advection processes which are responsible for the transmission of heat in the shallow sub-surface. Conduction is the diffusive transmission of solar-generated heat from the surface to the sub-surface in the absence of flowing groundwater while advection is defined as the heat carried by flowing groundwater in the sub-surface [*Anderson,* 2005]. Quantification of these heat transfer processes is based on Stallman's [1963] equation for the three-dimensional coupled transport of water and heat through saturated sediments. Time-series daily and seasonal temperature variations produce temperature profiles in the surficial zone (or depths less than 1.5 meters) that can be used to deduce surface and

groundwater interaction [*Anderson*, 2005]. Applying this fundamental principle to time-series temperature data from various depths in a shallow subsurface profile can be used to quantify the advective groundwater flux. With the advent of low cost, easily deployable temperature loggers, researchers have benefited greatly from using temperature profiles to study surface and groundwater interaction by applying it to a wide range of settings.

Using analytical or numerical solutions of Stallman's [1965] equation, many researchers have demonstrated the utility of thermal streambed temperature profiles to understand surface and groundwater interactions [*Constantz*, 2008; *Constantz et al*., 2013; *Rau et al*., 2012; *Briggs et al*., 2014; *Constantz et al.*, 2016].

The benefit of using the analytical solution for groundwater discharge to streams has been demonstrated for a variety of environments. Bredehoeft and Papadopulos [1965] provided an analytical solution to Equation 1 for the one-dimensional vertical flow of water through the saturated streambed while others have validated it by comparison with direct measurements from seepage meters [*Schmidt et al*., 2007; *Jensen and Engesgaard*, 2011; *Briggs et al*., 2014]. Additionally Lu and Ge [1996] extended the analytical solution by adding a source/sink term to account for hyporheic flow which is negligible when less than 10% of the vertical flow. Bhaskar et al. [2012] verified that the analytical solution was capable of detecting hyporheic flow while Hatch et al. [2006] shows that groundwater flux could be determined from changes in amplitude and phase shift of the diurnal temperature signal with depth.

Healy and Ronan [1996] provided a numerical solution to Equation 1 for determining the flow of water and heat through the variably saturated streambed in one or two dimensions (VS2DH). The validity of VS2DH was first confirmed by estimating recharge in a Nevada stream [*Ronan et al*. 1998]. More recently, Essaid et al. [2008] applied thermal methods to four different stream reaches and reported the VS2DH numerical results agreed well with seepage meter estimates. Briggs et al. [2014] compared VS2DH, analytical, and seepage meter estimates for a river in Massachusetts, reporting VS2DH and seepage meter estimates agreed well but discrepancies were evident when compared to the analytical results.

More recently, electrical resistivity (the inverse of conductivity) methods have been used to quantify advective groundwater fluxes. The premise behind this method is that most minerals in the subsurface are poor conductors of electricity and ionic fluids occupying pore spaces are electrically conductive. Temporal changes in conductivities have been associated with zones of groundwater flux [*Nyquist et al*, 2008] and specific discharge rates have been estimated using a salinity mass balance approach [*Bighash and Murgulet*, 2015; *Dimova et al*., 2012].

Time-series decomposition [*Cleveland et al*., 1990] was proposed as an alternative approach for analyzing thermal profiles in the streambed by decomposing (separating) the temperature into three components representing the annual temperature trend, a seasonal component representing heat conduction, and a random component representing

advection. It is assumed that finding lag correlations between the random components among different depths in the temperature profile would allow direct estimation of advective flux. Figura et al. [2015] used time-series temperature decomposition to predict future groundwater temperature changes in Switzerland by finding the temperature signal travel time between the de-trended seasonal components of air and groundwater temperatures while Shamsudduha et al. [2009] used the annual trend and the de-trended seasonal components to characterize long and short term trends in groundwater levels in Bangladesh. However, to my knowledge no research has attempted to estimate the advective groundwater flux using the random component

1.2. Unique Hydrology and Ecology of Texas Coastal Low-Flow Streams.

For the purpose of the study, Texas low-flow coastal streams are defined as streams whose headwaters originate in relative close proximity to the coast (i.e. approximately 50 km). The majority of Texas coastal streams and their tributaries are ephemeral however a small number have perennial flow. Perennial stream flow in the main stems of coastal low-flow streams generally results from springs and/or municipal wastewater discharge and a small fraction due to groundwater discharge where the majority of the latter is considered to occur as bank storage releases after storm events [*TCEQ*, 2005]. These coastal streams channels are generally poorly defined and are shallowly entrenched into the low permeability clay rich marine sediments of the Beaumont Formation, which were deposited on the shallow continental shelf and sub-aerially exposed in recent geologic

time as sea levels subsided. Texas coastal stream watersheds are characterized by nearly flat topography and consequently very low surface-water gradients [*TCEQ*, 2005]. Coastal streams are also affected by fluctuating tides, the effects of which can be increased due to wind velocity and direction, which under certain conditions help to drive sea-water further upstream [*Nicolau*, 2001]. The combined effects of fine-textured low-permeability sediments, tidal fluctuations, and low stream gradients make examining surface and groundwater interactions in these coastal streams particularly challenging.

The ecology of streams can be greatly influenced by surface water exchanges with groundwater. However, surface and groundwater in Texas coastal low-flow streams are typically moderately-saline to saline, therefore the number of species of organisms generally differ only in population density from the headwaters to the mouth of the stream [*Nicolau*, 2001].

1.3. Research Objectives.

The main objective of this study is to determine if the decomposition method applied to temperature time-series data can be used with confidence in deriving groundwater discharge rates to a low-flow stream in a semi-arid area. A combination of analytical, numerical, and electrical resistivity methods were employed to validate the proposed method by comparing groundwater flux estimates.

2. Data and Methods.

2.1. Study Site

The study site (Figure 1) is located in the Oso Creek watershed, adjacent to the Texas Gulf Coast near Corpus Christi. Oso Creek begins west of Corpus Christi and flows appoxiamtely 40 kilometers (km) where it discharges to Oso Bay. The main stream flows year round mainly due to municpal wastewater discharge while its tributaries are ephemeral and combined they drain an area of approxiamtely 600 square km (km^2) [*Ockerman and Fernandez,* 2010]. The relief in the basin is relatively low with an average gradient of 0.7 meters (m) per km [*Ockerman and Fernandez,* 2010]. The basin is characterized by unconsolidated low permeability clays and muds of the Beaumont Formation [*Bureau of Economic Geology,* 1975]. The mean annual temperature in the region is 21.9ºC and the average annual precipitation is 83.6 cm [*Ockerman and Fernandez,* 2010].

Temperature data was collected from 17 sites in the Oso Creek watershed. Of the 17 original sites only 3 were selected along Oso Creek, site SB-GW08, SB-GW19, and SB-GW04 (Figure 1) based on continuous/consistent time-series data. The site used in this analysis (SB-GW08) was selected given its proximity to the USGS stream gauging station #08211520 and its location outside the tidal influence as well as constant water flow.

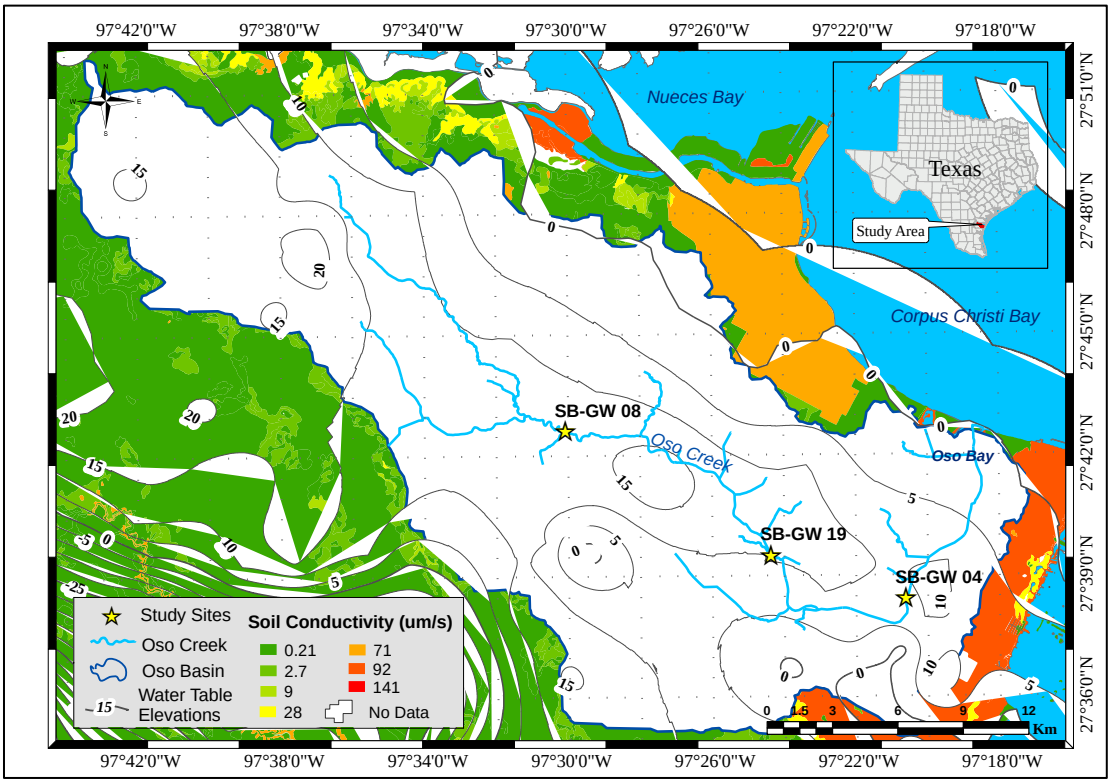

Figure 1: Geographic location of Oso Creek and study sites. The color scheme represents soil electrical conductivity and the black-labeled contour lines are the water table elevations. Site SB08 (SB-GW08) was the final site selected for this study.

2.2. Data Acquisition

Temperature data was collected from five temperature loggers installed at each site. Four of the temperature loggers are installed vertically in a profiler inserted into the streambed. The temperature profiler is constructed from 5.1 cm O.D. PVC pipe with a length of 150 cm fitted with four Maxim Integrated DS1922L iButton temperature loggers. 16.25 mm holes were bored in the PVC pipe and spaced at 0.0 m, 0.33 m, 0.66 m and 1.0 m intervals along the length of the profiler, the loggers were inserted into the holes and epoxied into place. The profiler was inserted vertically into the streambed such that the

uppermost logger (0.0 m) is situated approximately 5 cm above the sediment-water interface (Figure 2) and the loggers were set to record data at 15 minute intervals. The fifth logger is placed in a nearby groundwater well (Figure 2) and is set to record at the same interval. Data for the SB08 site was collected from June of 2009 to May of 2010.

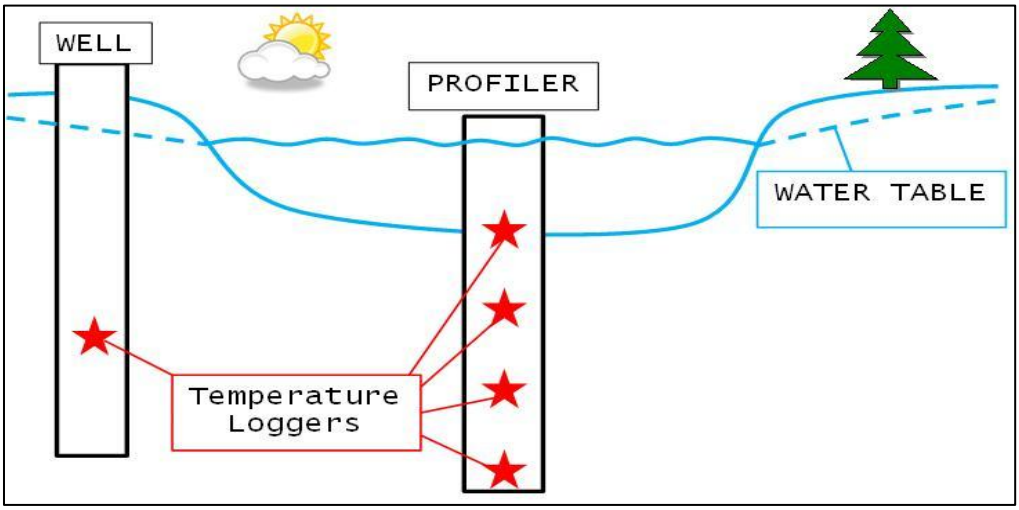

Figure 2: Generalized stream cross-section showing logger placement. (Not to scale)

Porewater, saturated streambed sediment, and surface water samples were collected for resistivity analysis using a resistivity test box (RTB). The RTB design is discussed in in the Geophysical Method section (2.4.4). Porewater was collected below the stream by means of a 5.1 cm x 1.5 m PVC well point with a 10 cm screened interval and 0.25 mm slots (Campbell Manufacturing BBP200-5). Because of the fine sediments at the study site, conventional methods of collecting porewater samples are often confounded by

clogging of the screen when attempting to force water out of the formation or by simply inserting extraction tools into the sediment.

To minimize clogging, a balloon was attached to a 2 m length of flexible poly-vinyl tubing with a valve attached at the opposite end and then inserted into the well point. The balloon was then inflated to seal the pores in the well point screen prior to insertion into the streambed. The well point was inserted by hand until resistance was felt at approximately 70 cm below the streambed and the exposed end of the pipe was sealed and allowed to stabilize for 48 hours. After stabilization, the balloon was deflated and the tubing assembly removed and the pipe was fitted with a vented cap to prevent contamination and pressure buildup in the pipe. Water was allowed to migrate naturally into the pipe for a period of 6 days after which the porewater was extracted.

Porewater samples were collected in a clean container for transfer to the RTB. No abnormal stream stage events occurred during the collection period that would cause contamination from surface water. Surface water and streambed sediments were collected by grab sample and placed in clean intermediate containers for transfer to the RTB. Resistivity values were determined using the RTB and a Fluke Model 87 digital volt-ohm meter.

2.3. Raw Data Pre-processing with R

Temperature data at the 17 sites was collected from mid-June 2009 through mid-May of 2010 resulting in 68 individual time-series consisting of approximately 32,600 records each. The length of the records varied due to the logistics of deploying and retrieving the temperature loggers from the various sites throughout the entire Oso Creek Watershed. The raw temperature data was compiled in a data base for later processing with R open source statistical software. Before any analysis of the raw data could begin the data needed to be extracted from the data base (Appendix A1.1-A1.2) and placed in an R recognizable format for ease of processing (Appendix A1.3-A1.4). Appendix A includes the scripts used in processing the data. The following text briefly outlines the general steps to process the data from one profiler. Data from the remaining 16 profilers was processed in a similar fashion.

First a table was created in R for the individual profiler where each row represents one record arranged chronologically and five columns representing timecode and temperatures at 0.0, 0.33, 0.66 and 1.0 meters. Next the timecode was arranged into an R recognizable format. The timecode of each record was arranged by the following convention: year, month, day, hour, minute and second (Appendix A1.3). Data was then exported for further processing (Appendix A1.4).

Because the individual sensors in each profiler started recoding data at slightly different times, the 15-minute time records did not correspond between the four sensors of each

profiler. A function was developed to automatically round the timecode to the nearest 15-minute interval creating a new data frame, which was then checked for corresponding 15-minute intervals (Appendix A2.4).

Due to sensor failure or other unforeseen circumstances some temperature records were missing or were noticeably above or below the expected temperature range. The function "fix.missing" was applied to automatically scroll through the data looking for NA values. Once identified, the missing value is replaced by the previous day's temperature value corresponding to the same time (Appendix A2.7-A2.11). To fix the out-of-range values a script was created that allowed scrolling through time averaged weekly plots (Appendix A3.1) of the temperature data and visually inspect for suspect data (Appendix A3.6). A user-defined time determines the length of time the plot is displayed (Appendix A3.5).

The temperature limit used to identify flawed data was set at a +/- 1.0 ºC, since it was expected that this amount of change in a 15 minute period is abnormal and therefore, warranted replacement (Appendix A3.2). Out-of-range data is detected and the flawed data is replaced with an "x" (Appendix A3.7). Next the data is listed to visually determine the record number associated with the "x" (Appendix A3.8). The "x" is then manually replaced with NA (Appendix A3.9). The function, "fix.missing" is then run again to replace the NA with the previous day's value (Appendix A3.10). Once the missing and outlier data have been replaced, plots for each sensor depth were visually checked for consistency and then merged into the original data set (Appendix A3.11-

A3.13). Duplicate records sometimes resulted from merging the data sets. To overcome this, a function was created to check for and remove duplicate records (Appendix A4.2-A4.3). After removal of duplicate records the data is again checked for consistency and then exported as filtered data (Appendix A4.4-A4.8).

The filtered data set was then merged with USGS stream discharge data, based on time, to enable plotting discharge with temperature data and look for correlations between high discharge events and outliers in the random component. The new data set was again checked for duplicate records and plotted for visual inspection (Appendix A5.1-A5.10). The final preprocessing steps entailed converting the filtered data set into an R time-series class with a frequency of one day (96 records) for further analysis by the various methods utilized in this study (Appendix A6.1-A6.5).

2.4. Data Analysis

2.4.1. Analytical Method: Type Curves

Stallman [1963] suggested that subsurface groundwater temperature profiles could be used to estimate groundwater flow. He further recognized that groundwater temperatures when used in conjunction with hydraulic head data could be used to estimate the hydraulic conductivity of the sediments. Following this reasoning he proposed a three-dimensional conduction-advection equation (Equation 1) describing the flow of heat and fluid in the sub-surface;

$$K_T\left[\frac{\partial^2 T}{\partial x^2}+\frac{\partial^2 T}{\partial y^2}+\frac{\partial^2 T}{\partial z^2}\right]-C_w\left(v_x\frac{\partial T}{\partial x}+v_y\frac{\partial T}{\partial y}+v_z\frac{\partial T}{\partial z}\right)=C_s\frac{\partial T}{\partial t}, \quad (1)$$

where K_T is the thermal conductivity of the bulk streambed sediments in W m^{-1} $^oC^{-1}$, T is temperature in ^{o}C at points x, y and z, C_w is the product of specific heat and density of water and termed the volumetric heat capacity with units of J m^{-3} $^oC^{-1}$, v is the fluid velocity in the x, y, and z directions with units of m s^{-1}, C_s is the product of the specific heat and density of the saturated sediments and termed the sediment volumetric heat capacity with units of J m^{-3} $^oC^{-1}$, and t is time in seconds. The first term on the left of Equation 1 accounts for the three-dimensional conduction of heat in the subsurface with respect to time as a function of thermal properties of the sediment. Similarly, the second term on the left describes the three-dimensional advective flow of heat in the subsurface with respect to time as a function of thermal properties of the fluid. The term on the right describes the change in temperature of the sediments with respect to time as a function of the volumetric heat capacity of the saturated sediments.

Stallman [1965] later extended his work to derive a one-dimensional steady state advection-conduction equation for vertical flow in the subsurface. Equation 2 formed the foundation for the use of heat as a tracer of groundwater flow [*Constantz*, 2008].

$$\frac{K_T}{C_s}\frac{\partial^2 T}{\partial z^2}-\frac{qC_{\mathrm{w}}}{C_s}\frac{\partial T}{\partial z}=\frac{\partial T}{\partial t} \quad (2)$$

In Equation 2, q is specific discharge with units of ms^{-1} and z is the depth below the streambed in the direction of water movement in meters. This equation can be used to calculate GW temperature T at any depth z at any time t. All other variables are the same as outlined previously for Equation 1. The first term on the left hand side of the equation represents heat conduction while the second term represents advection. Analyzing Equation 2 reveals that when q is large, heat transfer by advection will dominate.

Conversely for small values of q the transfer of heat by conduction will dominate which inhibits the determination of small water fluxes [*Rau* et al., 2012]. In the absence of any vertical groundwater flow (when q equals zero), the second term on the left vanishes and Equation 2 reduces to the purely conductive state:

$$\frac{K_T}{C_s}\frac{\partial^2 T}{\partial z^2} = \frac{\partial T}{\partial t} \tag{3}$$

These equations are only valid if the following circumstances are met [*Stallman*, 1965].

- Water flow is steady-state and parallel to the z axis.
- Heat propagates parallel to the z axis
- Thermal parameters of the water and matrix are temporally and spatially constant.
- The temperature of the pore water is equal to the temperature of the matrix.

Numerous researchers have developed analytical solutions and numerical models based on Stallman's equations. Bredehoeft and Papadopulos [1965] were some of the earliest researchers to recognize the utility of Stallman's work and proposed an analytical

solution to quantify vertical groundwater flow. Their analytical equation for advection and conduction vertically through streambed is as follows:

$$\frac{T_z - T_{sw}}{T_{gw} - T_{sw}} = \frac{exp\left[N_{pe}\left({}^{z}/_{L}\right) - 1\right]}{exp\left(N_{pe} - 1\right)}, \tag{4}$$

where T_z is the temperature at any depth z in ºC, T_{sw} is the temperature of the surface water in ºC, T_{gw} is the temperature of the groundwater in ºC, L is the vertical distance between surface (T_{sw}) and groundwater (T_{gw}) temperatures in meters, z is the distance between surface temperature (T_{sw}) and the point being estimated (T_z) and N_{pe} is the thermal Peclet number given by:

$$N_{pe} = \frac{q_z C_w L}{K_T}. \tag{5}$$

The thermal Peclet number describes the ratio of advection to conduction. Bredehoeft and Papadopulos [1965] demonstrated using type curves (Figure 3) that positive Peclet values indicate losing stream conditions while negative values indicate a gaining stream. Rau et al. [2012] extended this reporting that advection dominates when thermal Peclet absolute values are greater than one ($\left|N_{pe}\right| > 1$) while values less than one ($\left|N_{pe}\right| < 1$) are conduction dominated. Following this reasoning it may be difficult to ascertain which process dominates for Peclet values close to one.

To calculate the flow specific discharge q at a specific point in time using the analytical solution, a minimum of three subsurface temperature values are required, namely T_z, T_{gw}, and T_{sw} [*Schmidt* et al. 2007]. Figure 4 is a conceptual view describing the application of the analytical method. Field data of $\frac{T_z - T_{sw}}{T_{gw} - T_{sw}}$ is plotted against the depth factor z/L which are then superimposed over type curves (Figure 3) for various values of N_{pe} developed by Bredehoeft and Papadopulos [1965]. The value of N_{pe} is determined from the type curve that best matches the field data. The specific discharge q is then calculated by

$$q = \frac{K_T N_{pe}}{C_w L}. \tag{6}$$

Temperature data was collected at four different depths/elevations (one in the stream and three in the streambed) in the vertical streambed profile making it possible to estimate the vertical specific discharge during the summer and winter periods at the 33 cm and 66 cm depths (see Figure 4). The daily surface temperature at 0.0 cm was used as the upper boundary (T_{sw}) and the 100 cm depth temperature as the lower boundary (T_{gw}). Schmidt et al. [2007] used the average surface and groundwater temperatures as boundary conditions. Jensen and Engesgaard [2011] chose the average maximum surface temperature as the upper boundary and a constant groundwater temperature for the lower boundary. For this study the instantaneous daily surface and groundwater temperatures were used as boundary conditions to obtain a better estimate of q throughout the period and thus enable direct comparison to the numerical model results.

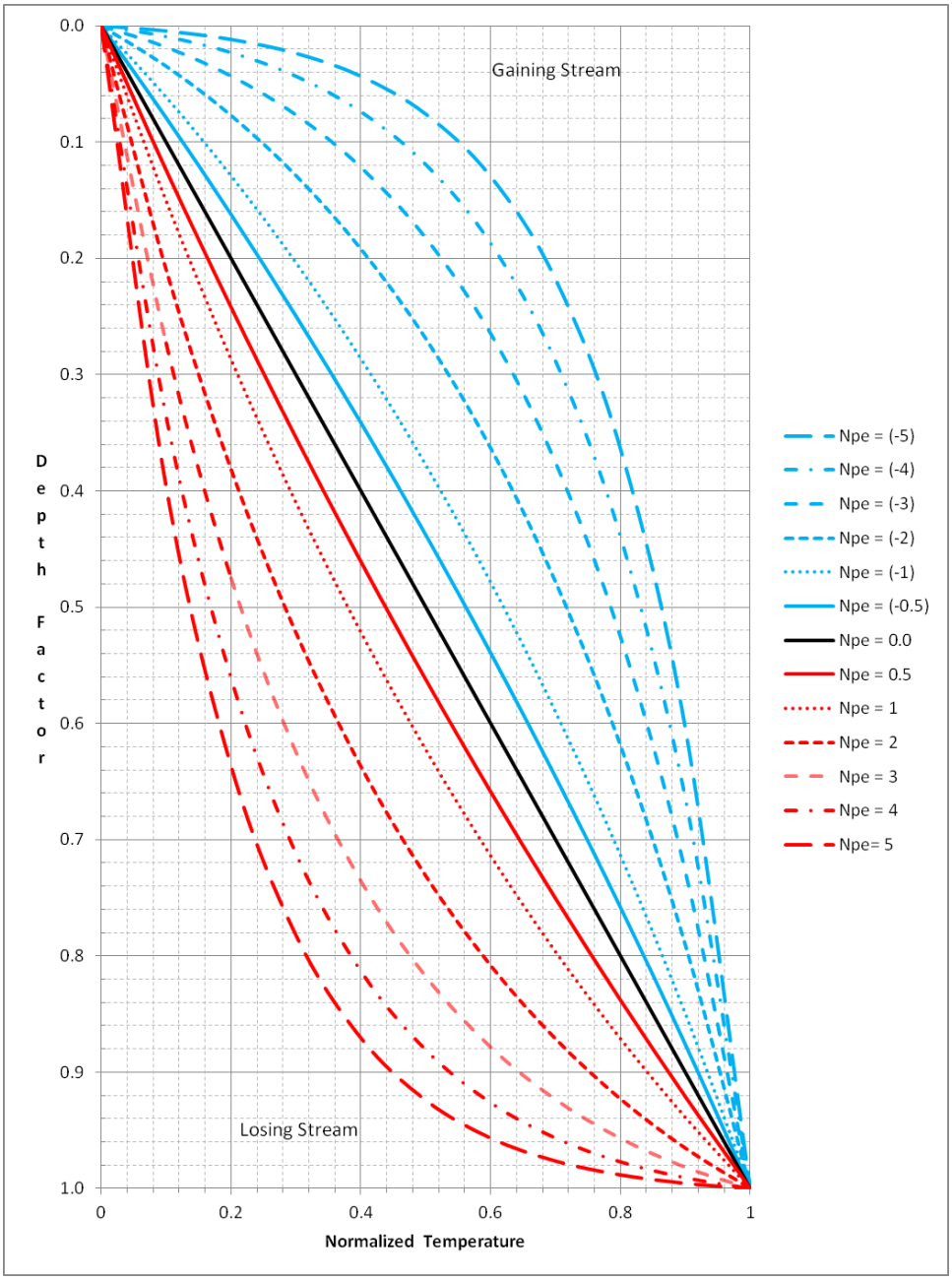

Figure 3: Type curves plotted for values of N_{pe} ranging from 5 to -5. The black linear plot represents pure conduction. Increasing groundwater discharge bends the plot progressively upward and increasing surface water discharge into the stream sediments bends the plot progressively downward. Modified from Bredehoeft and Papadopulos [1965].

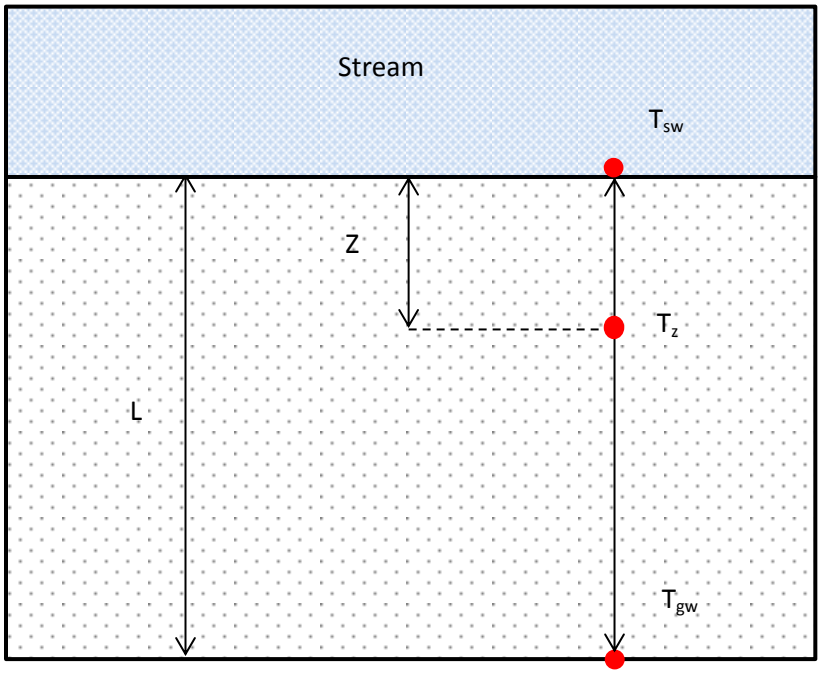

Figure 4: Conceptual view of a stream and the underlying sediments describing the analytical method boundary conditions and relative locations of the temperature inputs.

The analytical solution outlined above is most accurate during periods with reasonably steady temperatures, which occur mainly during the summer and winter [*Schmidt* et al., 2007; *Jensen and Engesgaard*, 2011; *Anibas* et al. 2009]. Therefore the time series was divided into periods considered to represent summer and winter where the temperature fluctuations are the most stable. For this study, steady conditions are defined as periods when the temperature of any sensor does not frequently equal the temperature of another sensor. The effect of converging temperatures at different depths can be seen when looking at the left side of Equation 4. As the temperatures converge the values obtained

from this term can result in extremely large or small numbers or division by zero errors. These values can significantly skew the value of N_{pe} obtained from the type curve match and result in unrealistic estimates of specific discharge. Therefore periods of time when the temperature profiles exhibited this behavior were omitted from calculations [*Schmidt* et al., 2007; *Jensen and Engesgaard*, 2011; *Anibas* et al. 2009].

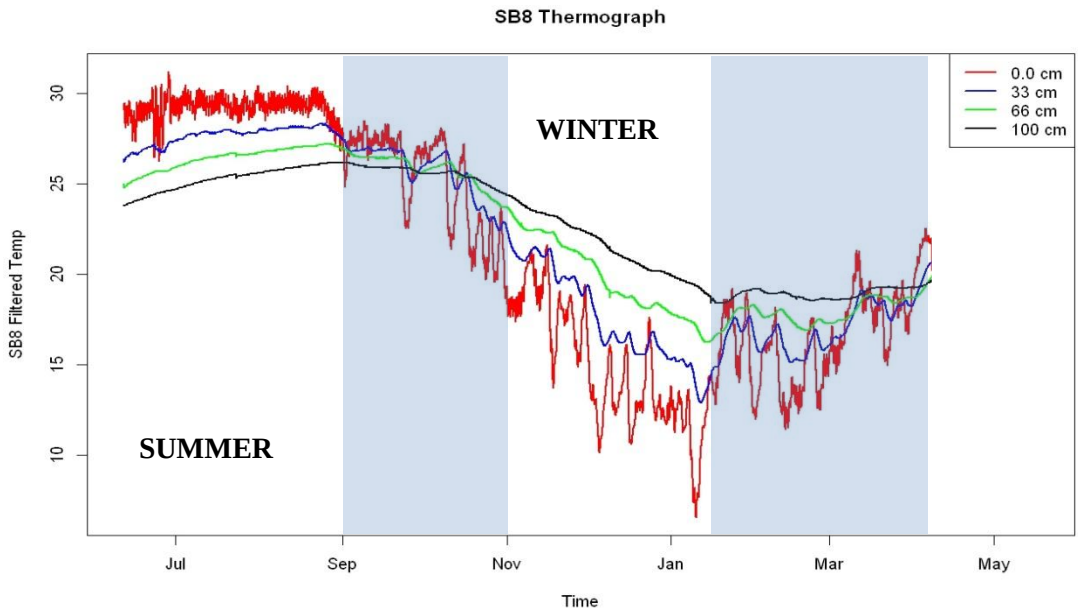

Figure 5: Thermograph of temperatures for all depths for site SB8 showing summer and winter periods. Shaded areas represent periods not used in the calculations.

Steady periods were determined by visually inspecting the thermographs. The temperature profiles were reasonably steady from the beginning of the record on June 11, 2009 through September 1, 2009 and began to decrease significantly after. The summer

period is considered to begin June 18, 2009 and continue through August 28, 2009. The winter period is considered to begin after September 1, 2009 and continue until January 14, 2010 (Figure 5). For comparison purposes this convention is also used in the numerical method.

2.4.2 Numerical Method: VS2DH

VS2DH represents an alternative to the analytical solution outlined previously for estimating groundwater flow. VS2DH is a numerical model developed by the U.S. Geological Survey (USGS) that simulates the flow of energy and water in the subsurface [*Healy and Ronan*, 1996]. The model solves coupled energy and water flow equations in one or two dimensions. The energy equation (Equation 7) solved by VS2DH is the three-dimensional form of the advection-dispersion equation for the transfer of thermo-mechanical energy [*Ronan* et al., 1998; *Constantz*, 2008]:

$$\frac{\partial[\,\theta C_w + (1-\phi)C_s]T}{\partial t} = \nabla\cdot K_T(\theta)\nabla T + \nabla\cdot \theta C_w D_H \nabla T - \nabla\cdot \theta C_w T q + Q C_w T_s \quad (7)$$

where t is time in seconds, θ is the moisture content by volume, C_w is the volumetric heat capacity of water in J m^{-3} $^oC^{-1}$, ϕ is porosity, C_s is the heat capacity of the sediments in J m^{-3} $^oC^{-1}$, T is temperature in ^{o}C, K_T describes the three-dimensional thermal conductivity of the saturated sediments in W m^{-1} $^oC^{-1}$, D_H accounts for three-dimensional

hydrodynamic dispersion with units of m^2 s^{-1}, q is water specific discharge in ms^{-1}, Q is the rate of the water source in s^{-1} and T_s is the temperature of the water source [*Healy and Ronan*, 1996; *Constantz*, 2008].

The term on the left side of Equation 7 describes the change in temperature of variably saturated sediment over time. The first term on the right of Equation 7 describes heat conduction, the second term accounts for thermo-mechanical dispersion through the sediments, the third term represents heat advection, and the fourth term represents heat sources or sinks into or out of the model [*Constantz*, 2008]. The numerical solution incorporates heat source/sink and thermo-mechanical dispersion terms into the equation, which do not appear in the analytical solution. The heat source/sink term accounts for time varying temperature boundary conditions and variable water flow rates whereas the analytical solution assumes steady state boundary conditions and a constant flow of water. As opposed to the analytical solution which assumes straight flow and transport paths for water and heat through the porous media, the thermo-mechanical dispersion term accounts for tortuous/preferential paths caused by subsurface heterogeneities.

Water flow through the subsurface is described by Richard's equation with the total head form solved by VS2DH as follows [*Constantz*, 2008]:

$$C(h,x)\frac{\partial h(x,t)}{\partial t} = \nabla[K(h,x)\cdot\nabla H(x,t)], \tag{8}$$

Where C is the specific moisture capacity in m^{-1}, h is the water pressure in m, x is length in m, t is time in s, K is the hydraulic conductivity in ms^{-1} and H is the total head in m [*Constantz*, 2008].

VS2DH first calculates the pore water specific discharge (Equation 8) which is then used to determine heat advection and dispersion (Equation 7) [*Ronan et al.,* 1998]. This process is repeated until the change in specific discharge between iterations converges on a predetermined value. VS2DH was implemented through the USGS graphical user interface 1DTempPro [*Voytek, et al.,* 2014] which allows for manual calibration of the coupled energy and flow solutions from VS2DH to measured thermal profiles in one-dimension and it is particularly well suited for analyzing vertical flux when no head data is available [*Voytek, et al.,* 2014, *Koch et al.,* 2015]. Since data were available only in vertical direction and no head measurements were acquired, 1DTempPro was a logical choice for analyzing the data.

The specific discharge is calculated through 1DTempPro analysis using specified parameters and the best fit of observed and calculated temperature data. Before analysis the with 1DTempPro the filtered temperature data from all four levels of the SB8 profiler and their associated dates and times were exported from R and compiled into a comma delimited file following the format suggested by Voytek, et al. [2014]. The temperatures of the upper (0.0 cm) and lower (100 cm) sensors were used to define the models upper and lower boundaries respectively and the temperature at the 33 and 66 cm depths were

used for model calibration. Fixed parameter values were used in the calibration of specific discharge. The calibration parameter, specific discharge, was determined from the analytical solution results and an initial value of -7 mm d^{-1} was used. Model calibration was achieved by adjusting the value of specific discharge until a best fit between modeled and observed temperature was achieved. Since the temperature logger precision used in this study is 0.0625 ºC, the RMS target (a measure of the goodness of fit of modeled versus observed data) was chosen around this value [Briggs et al., 2014; Koch et al, 2015].

2.4.3. Statistical Method: Seasonal-trend decomposition (STL)

Seasonal-trend decomposition using Loess (STL) decomposes a temperature time series (Y_t) into trend (T_t), seasonal (S_t) and random (R_t) components [*Cleveland* et al., 1990]:

$$Y_t = T_t + S_t + R_t. \quad (9)$$

Carslaw [2005] used the decomposition trend and seasonal components to analyze monthly and annual trends in ozone levels in Ireland while Jiang et al. [2010] used the same components to model and predict temporal and spatial changes in land surface vegetation. However, no evidence has been found using analysis of the random component.

The hypothesis is that STL can separate the conductive and advective components of heat transfer. The vertical conduction of heat in the streambed is assumed to result from

periodic diurnal temperature fluctuations at the surface, therefore the conduction can be modeled by the seasonal component (S_t). Conversely it is assumed that heat advection is not periodic and can be represented by the random (R_t) component. The objective using the STL method is to directly derive a flux using the random components between two depths in the streambed. Since it is assumed that outliers in the random component will characterize periods of advection; the time lag between outliers is then divided by the distance between the two depths to directly achieve a velocity which can be converted to specific discharge.

STL decomposition uses locally weighted regression (Loess) to model the seasonal and trend components based on observed data. For a specific record in the time-series, Loess applies a weighted value to every neighboring record in a local subset of data based on its distance from the record being scrutinized [*Cleveland* et al., 1990]. For accurate modeling of the data, it is critical that the number of records included in the local subset match the fundamental frequency in the data (e.g. daily, weekly, or monthly) [*Cleveland* et al., 1990]. Because the frequency in this study is daily, a subset size of 96 records (the number of 15 minute records in one day) was used. Local subsets larger or smaller than the frequency in the data circumvent the decomposition procedure and result in too much or too little temperature information in the random component [*Cleveland* et al., 1990] which would adversely affect any flux calculations.

The Loess method is applied in a series of recursive inner and outer loops to extract the trend and seasonal components. The inner loop applies Loess to a daily subset (96 records) of the time-series to estimate the seasonal component and is then applied again to the daily subset to estimate the trend component [*Cleveland* et al., 1990]. Using the outer loop, the locally weighted fitted values for the trend and seasonal components are computed. The resulting values will be used in the next iteration of the inner loop to better estimate the trend and seasonal components. Convergence is typically attained in less than 10 iterations of the outer loop [*Cleveland* et al., 1990]. Upon convergence the trend and seasonal components are removed from the original time-series where the random component (R_t) is given by:

$$R_t = Y_t - S_t - T_t \tag{10}$$

STL was implemented using R open source statistical software.

2.4.4 Geophysical Method: Electrical Resistivity

Resistivity profiles (tomographs) were acquired with an Advanced Geosciences, Inc. (AGI) SuperSting® R8/IP eight channel induced polarization resistivity instrument [AGI unpublished material]. Resistivity tomographs were analyzed to identify zones of interaction between surface and groundwater by comparing the SuperSting resistivity (ERT) values to test box resistivity (TBR) values of surface and groundwater and saturated streambed sediments acquired from field samples using a fabricated resistivity test box. Since the ERT-derived resistivities are indirect measurements and the TBR are

direct measurements and since it is assumed that the saturated sediments, surface water, and groundwater have different electrical conductivities (inverse of the resistivity) [*Samouelian* et al., 2005], the TBR data will facilitate identification of the composition of contrasting zones in the ERT tomography Using tomographs acquired at different times, the change in bulk resistivity over time in the zones of interest was used to estimate flux rates.

The SuperSting is an 8-channel instrument capable of estimating the resistivity at 8 depths simultaneously which greatly increases acquisition time. Data is acquired by means of a multi-conductor cable containing 56 hard graphite electrodes spaced 2 meters apart resulting in an estimated imaging depth of 22 meters. Data was collected using an 8-channel dipole-dipole array where a pair of electrodes injects current and the voltage difference is measured by 9 electrodes comprising 8 pairs of potential electrodes [AGI unpublished material]. This sequence is repeated until all 56 electrodes have been utilized as determined by a user-created command file. To acquire resistivity data the cable is positioned in a straight line on the ground surface and the 56 electrodes are attached to stainless steel stakes driven into the ground. Collected resistivity data is processed using the 2D AGI EarthImager software, which uses a maximally smooth least squares algorithm to provide initial estimates of resistivity. The initial estimates are iteratively adjusted until a best fit model is obtained using the root mean square (RMS) error and L-2 norm values as indicators of best fit. In land-based surveys, high RMS and L-2 norm

values typically result from poor connections between the electrodes and the ground or the SuperSting injection current is near background levels in the subsurface [AGI unpublished material]. Ensuring good connections at the electrodes or increasing the injection current generally helps resolve these issues.

To verify the accuracy of analytical and mathematical techniques used in this study, ERT data were collected at the selected investigation site over a 3.5-hour time span on May 21, 2014. The cable was deployed perpendicular to the stream on a north-south trending transect with the 25th electrode placed on the streambed. During the inversion process, EarthImager assumes a flat ground surface therefore the spacing between electrodes is constant. However topographic relief essentially changes the spacing between electrodes which results in miscalculations. Due to surface irregularities at the study site the elevation of every electrode was surveyed and the derived terrain file was imported in EarthImager to minimize these errors.

TBR resistivity values were calculated directly using a fabricated resistivity test box. The dimensions for the TBR were determined by applying the definition of resistivity for an idealized cylinder [*Samouelian* et al., 2005].

$$\rho = R\left(\frac{S}{L}\right) \tag{11}$$

where R is resistance in ohms (Ω), L is the length in meters of the cylinder, and S is the cross sectional area of the cylinder in m^2. The inverse of resistivity is electrical

conductivity (σ) or specific conductance and is given by $\sigma = \rho^{-1}$ with units of Siemens per meter (S m^{-1}) [*Samouelian* et al., 2005]. The box was constructed of non-conducting plastic with a cross sectional area (S in equation 11) of 12 cm^2 and an inside length of 22 cm. An electrode is affixed to each end of the box and two electrodes are centered along the length of the box between the outer electrodes with a spacing of 12 cm (L in equation 11). Passing current through the two outer electrodes and reading the potential difference between the two center electrodes gives a direct resistivity value in Ω cm. These direct measurements are compared to the ERT derived resistivities and used as ground-truthing data and the only fundamental differences are spatial.

Time-difference inversion algorithms were used to calculate the percent difference in bulk resistivity between two consecutive images collected 3.5 hours apart using the AGI EarthImager software. EarthImager derives a time-difference inversion using the first and last ERT as the initial (base) and final (monitor) conditions image and produce an image representing percent change in bulk resistivity during the 3.5-hour time-span. Boxes representing the vertical area in m^2 of potential zones of surface water groundwater exchange were superimposed on the base, monitor and difference images [*Dimova* et al., 2012; *Bighash* and *Murgulet*, 2015]. Only those areas with percent changes exceeding the RMS error are selected for groundwater discharge estimates.

To reduce the effect of clay in resistivity measurements, porewater salinities were corrected using the formation factor (F^*) for water saturation of the sediments [*Lee* and *Collett*, 2006]:

$$F^* = a^* \phi^{-m^*} \tag{12}$$

Where ϕ is porosity and a^* and m^* are the clay corrected constants. Lee and Collett [2006] derived clay corrected constants using a least-squares fitting of log-porosity and log-resistivity values for sediments with clay contents up to 75%. The clay corrected constants for a^* and m^* are given as 1.09 and 1.70 respectively and assume a 75% clay content [*Lee* and *Collett*, 2006]. The clay corrected porewater resistivity (ρ_w^*) in Ω m is then calculated using the formation resistivity (ρ_f) in Ω m by:

$$\rho_w^* = \frac{\rho_f}{F^*} \tag{13}$$

Salinity (S) values for each superimposed zone are then calculated using:

$$S = 7.042 \rho_w^{*-1.0233} \tag{14}$$

Using Equation 3 allows the ERT derived porewater resistivity (ρ_w^*) is converted to salinity (in units of parts per thousand (ppt)) [*Manheim* et al., 2004]. Salinity (S) estimates for the zones in the base (S1) and monitor (S2) images, the volume of groundwater discharge (V_{gwd}) is calculated using a salinity mass balance approach as explained below:

$$V_{gwd} = V_{sal} \left[\frac{S1 - S2}{S2} \right] \tag{15}$$

The mass balance approach applies the conservation of both mass and salt principles. For steady-state conditions over a specified time, the groundwater discharge rate is calculated as the difference between the salinity inputs and outputs, neglecting dispersion (or diffusion). The mass balance is based on time-varying salinity concentrations at the study site. For a detailed description of this method refer to Dimova et al. [2012]. Equation 4 is based on the assumption that the entire volume of groundwater identified in the zones will eventually discharge into surface waters under hydrologic conditions favoring groundwater discharge to surface water (i.e. upward hydraulic gradients).

3. Results and Discussion

3.1. Analytical Method: Type Curves

Vertical groundwater specific discharge was calculated using the methods developed by Bredehoeft and Papadopulos [1965] (see Section 2.4.1 for details of this method). The normalized stream temperatures used to interpret the thermal Peclet number were calculated for each record to avoid errors caused by non-steady state boundary conditions resulting from daily and seasonal temperature changes [*Anderson*, 2005; *Schmidt* et al., 2007; *Anibas* et al., 2009; *Jensen and Engesgaard*, 2011; *Rau* et al., 2012]. The specific discharge was estimated at the 33 cm and 66 cm depths for the summer and winter periods. Thermal parameters used in the calculations were as follows: The thermal conductivity (K_T) of saturated clay was 0.837 W m^{-1} $^oC^{-1}$ [*Stallman*, 1965]. The

volumetric heat capacity (C_w) of water was 4.2 x 10^6 J m^{-3} $^oC^{-1}$ [*Constantz*, 2008]. The specific discharge results are given in Table 1.

Table 1: Analytical Method Estimated Specific Discharges

Period	q (mm d^{-1})	Depth (cm)	Flow Direction
Summer	6.9	33	Upward
Winter	1.7	33	Upward
Summer	6.5	66	Upward
Winter	4.3	66	Upward

The thermal Peclet numbers for summer and winter periods were all below one with a maximum value of 0.38 indicating conduction was primarily responsible for heat transfer into the streambed [*Anderson*, 2005, *Rau* et al., 2012]. The average specific discharges for the summer 33 and 66 cm depths were depth 6.9 mm d^{-1} and 6.5 mm d^{-1}, respectively and indicated that groundwater discharge was occurring. The average specific discharges for the winter 33 and 66 cm depths were depth 1.7 mm d^{-1} and 4.3 mm d^{-1}, respectively also indicating groundwater discharge. The specific discharge estimates obtained during the summer period for both depths were in relatively close agreement. The slightly lower specific discharges estimated during the winter could be explained by the higher stream stage during the winter period. The average stream stage in close proximity to the study

site was 1.5 m and 1.9 m for the summer and winter periods, respectively [*USGS*, 2015]. Higher pressure gradients resulting from higher stream stage could force water into the streambed, thus offset opposing flows [*Cox* et al., 2007, *Cuthbert and Mackay*, 2013] reducing the overall upward vertical component of groundwater specific discharge.

The idea that the flow of heat and water is strictly vertical is an assumption of the analytical one-dimensional solution. Violations of this assumption can lead to discrepancies in specific discharge at different depths when hyporheic and vertical flow occur simultaneously [*Jensen and Engesgaard*, 2011; *Bhaskar* et al., 2012]. Hyporheic flow occurs when stream water flows into the streambed sediments and then back to the stream [*Swanson and Cardenas*, 2010]. This non-vertical flow component may explain the differences in specific discharge with depth realized during the winter where the specific discharge at the 33 cm depth is roughly half of the specific discharge at the 66 cm depth. Bhaskar [2012] suggests that when one temperature sensor is in the hyporheic zone and stream discharge is higher relative to another point in time at the same location and depth, specific discharges estimated using the analytical method do not account for hyporheic flow and result in lower estimates at shallow depths typical of the hyporheic zone. For the Oso Creek study site, the average stream discharge for the summer and winter periods were 0.04 and 1.3 $m^3 s^{-1}$, respectively [*USGS*, 2015]. This higher stream discharge in winter likely explains the observed differences in groundwater specific discharge between the two depths and indicates that the shallow senor is located in the

hyporheic zone where horizontal exchange is likely to dominate under high flow conditions. Deriving a better estimate of the vertical specific discharge requires knowledge of the hyporheic to vertical flow ratio generally accomplished with additional temperature data acquired horizontally in relative close proximity to the vertical sensors [*Bhaskar* et al., 2012].

3.2. Numerical Method Results and Discussion: VS2DH/1DTempPro

The numerical solution was implemented using 1DTempPro for the one-dimensional case of vertical fluid flow through the streambed (see Section 2.4.2 for details of this method). Specific discharges were calculated at the 33 and 66 cm depths for summer and winter periods as described in the analytical section 2.4.1. Four fixed parameters were used in 1DTempPro. A sediment heat capacity (C_s) of 2.3×10^6 in Joules m^{-3} $^oC^{-1}$ was estimated using an experimentally derived dry bulk density of 2.2 grams cm^{-3} [*Lapham*, 1989, *Gealy*, 2007]. The value used for dispersivity (a) was 1.0 m [*Niswonger and Prudic*, 2003]. The experimentally derived average porosity (ϕ) was determined to be 0.64 [*Gealy*, 2007], and the thermal conductivity (K_T) of saturated clay was 0.836 (W m^{-3} $^oC^{-1}$) [*Stallman*, 1965]. Table 2 reports the final parameter values used as inputs for 1DTempPro. Values used for calibration of specific discharge ranged from ±20 mm d^{-1}.

Table 2: Parameters Used in VS2DH Modeling.

Description	Symbol	Units	Value	Source
Sediment Heat Capacity	C_s	J m^{-3} $^oC^{-1}$	2.3 x 10^6	Lapham [1989]
Dispersivity	α	meter	1.0	Niswonger and Prudic [2003]
Porosity	ϕ	–	0.64	Lab analysis
Thermal Conductivity	K_T	W m^{-1} °C^{-1}	0.836	Stallman [1965]

The summer 33cm depth shows a best-fit RMS of 0.076 °C which is slightly above the target value of 0.0625 °C (Figure 6) and simulation results indicate an upwelling specific discharge of 16 mm d^{-1}. The winter 33cm depth shows an excellent fit RMS of 0.057 °C (Figure 7) which is below the target value and indicated upwelling specific discharge at 3.5 mm d^{-1}. Figure 8 shows an excellent fit for the summer 66cm depth data with an RMS of 0.042 °C and indicating an upwelling specific discharge of 7.0 mm d^{-1}. The best fit RMS for the winter 66cm depth was 0.054 °C (Figure 9) and an upwelling specific discharge of 4.5 mm d^{-1}. The 1DTempPro results are listed in Table 3.

Table 3: 1DTempPro Model Results

Period	q (mm d^{-1})	Depth (cm)	Flow Direction	RMS
Summer	16.0	33	Upward	0.076
Winter	3.5	33	Upward	0.057
Summer	7.0	66	Upward	0.042
Winter	4.5	66	Upward	0.054

Similar to the analytical method results, the VS2DH estimates show that groundwater upwelling was occurring throughout both seasons at both depths with slightly higher specific discharge during the summer period (Table 3). Specific discharge estimates at all depths using the numerical method were slightly higher than those obtained using the analytical method, but vary with depth for both summer and winter. In particular the summer period numerically- estimated specific discharge values were markedly different between the 33 and 66 cm depths with magnitudes of 16 and 7 mm d^{-1}, respectively. This observation suggests possible heterogeneity in the streambed. However the analytical method results were in relatively close agreement at 6.9 and 6.5 mm d^{-1}, which would indicate overall homogeneity as also indicated by streambed core sample characterizations.

Another possible explanation for the discrepancies observed between the two depths during the summer period using the numerical method is non-vertical groundwater flow (i.e. hyporheic flow) [*Jensen and Engesgaard*, 2011; *Bhaskar* et al., 2012; *Voytek* et al., 2014]. As mentioned in the analytical section, the stream stage and discharge were both lower during the summer period resulting in steeper hydraulic gradients that may enhance the potential for groundwater discharge to the stream [*Cox* et al., 2007, *Cuthbert and Mackay*, 2013]. In addition Capuano and Jan [1996] showed that horizontal hydraulic conductivity in the Beaumont Clay sediments is 3 to 6 orders of magnitude larger than the vertical hydraulic conductivity. Thus horizontal flow likely dominates vertical flow and supports the non-vertical groundwater discharge to the stream assumption. The observation of numerous small seeps occurring at different elevations along the south bank of the creek also suggests preferential horizontal flow. The mixing of hyporheic flow and groundwater discharge can also be a factor when discrepancies in specific discharges occur at different depths [*Jensen and Engesgaard*, 2011; *Bhaskar* et al., 2012]. Shope et al. [2012] suggested that hyporheic mixing includes vertical surface and groundwater exchanges as well as lateral bank storage exchanges, a complex mixing scenario significantly violating the vertical flow assumptions of the one-dimensional model. Field observations during sediment core retrieval support the potential for hyporheic mixing. Minimal resistance was encountered when a 10.4 cm OD PVC pipe was inserted by hand to a depth in excess of 60 cm below the streambed revealing very loose sediment and the likely existence hyporheic mixing. Thus it is assumed that

hyporheic mixing is responsible for changes in specific discharge reported at different depths for both the summer and winter periods. However, the overall decrease in vertical specific discharge during winter is assumed to also be the result of gentler hydraulic gradients caused by higher stream stage levels described in the analytical methods section.

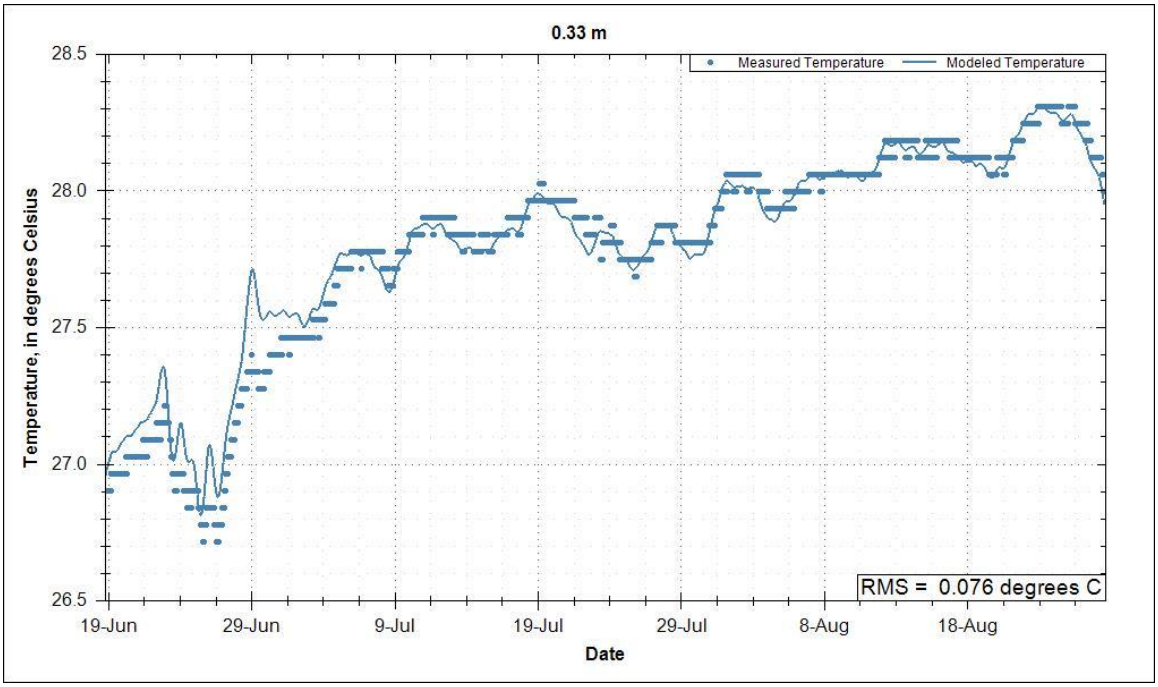

Figure 6: summer 33 cm; best fit of modeled versus measured (bold dots) temperature.

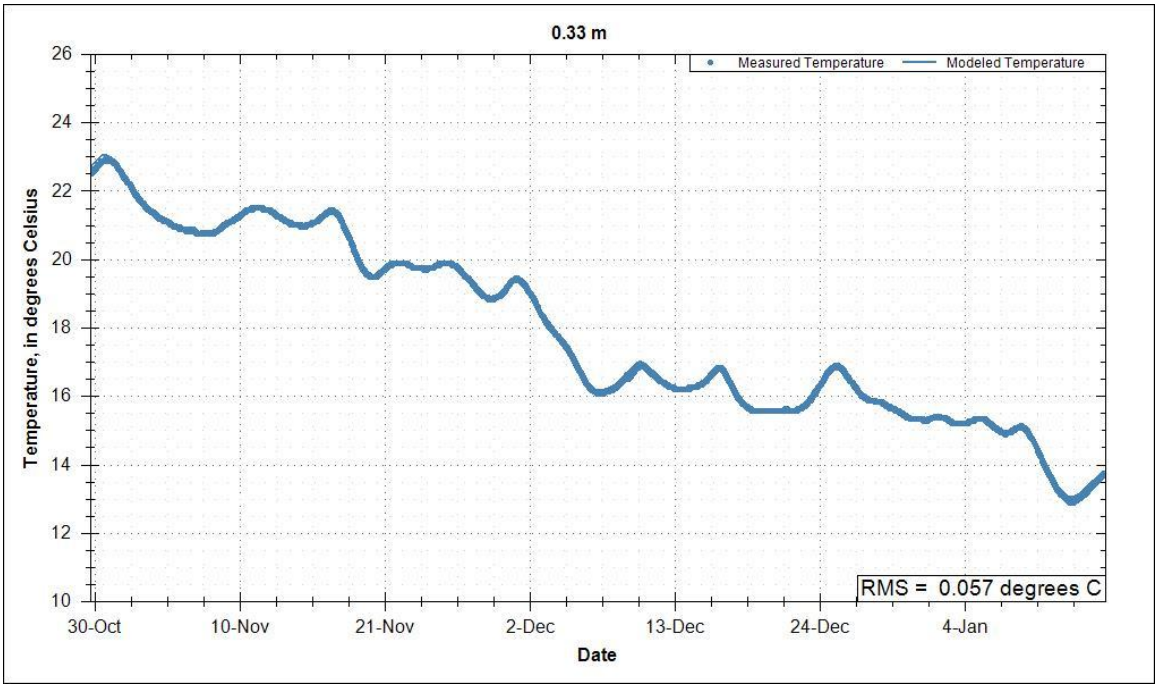

Figure 7: winter 33 cm; best fit of modeled versus measured (bold dots) temperature.

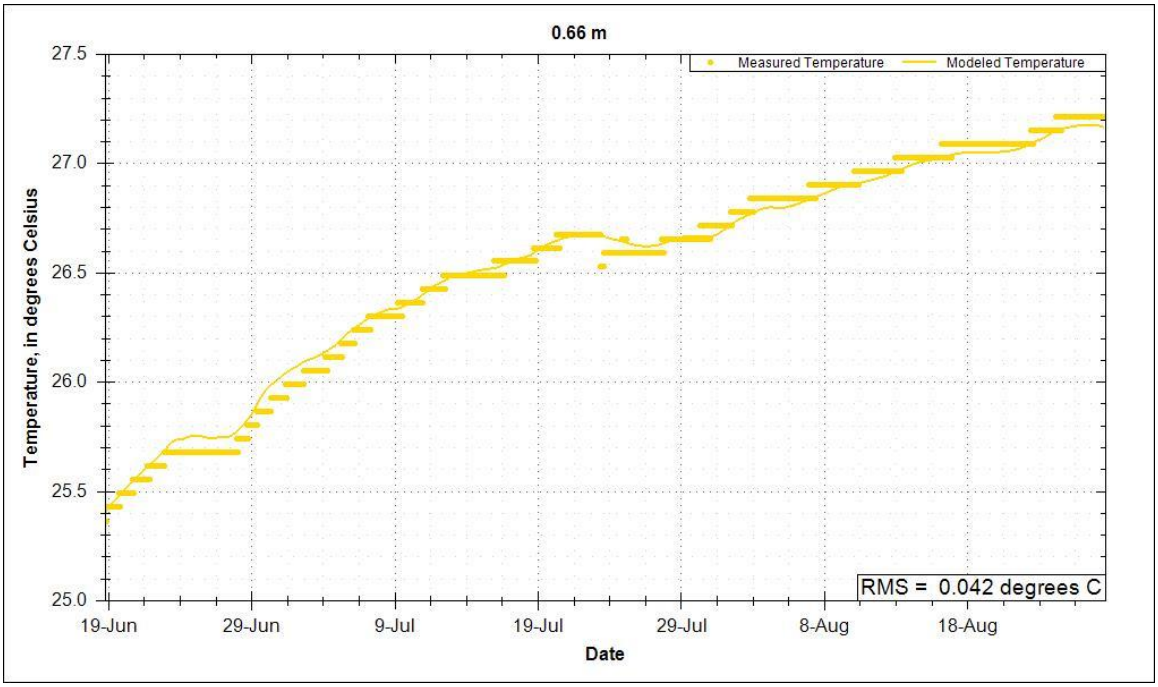

Figure 8: summer 66 cm; best fit of modeled versus measured (bold dots) temperature.

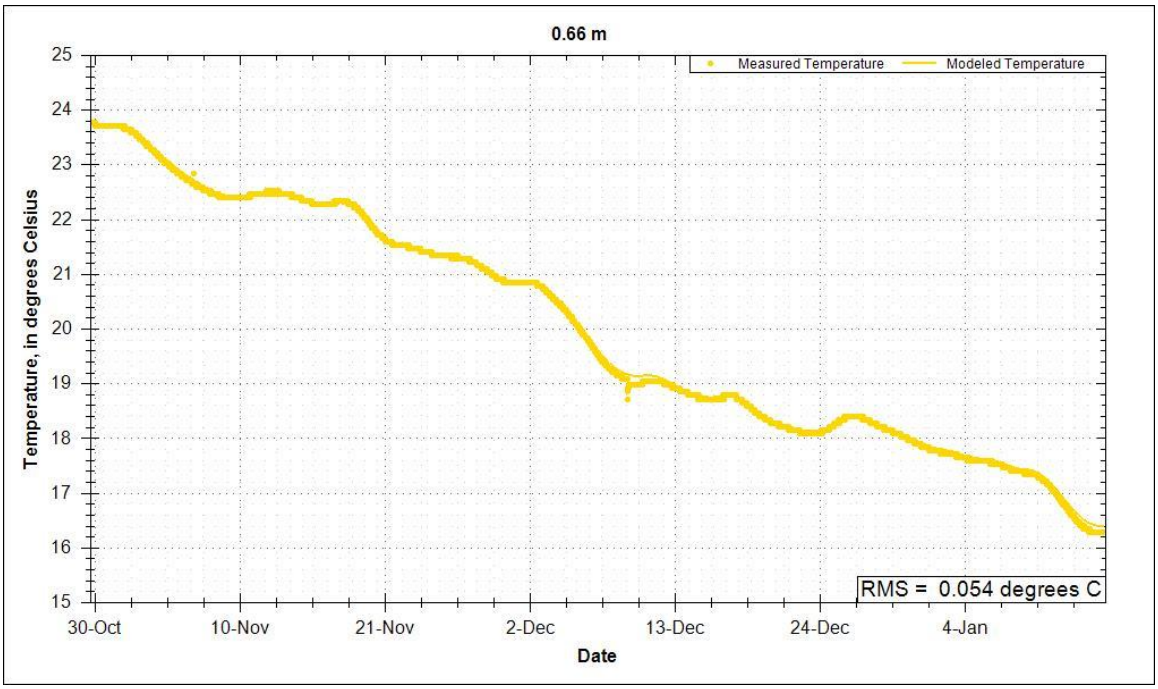

Figure 9: winter 66 cm; best fit of modeled versus measured (bold dots) temperature.

3.3. Statistical Method: STL

STL decomposition was applied to all levels of the SB08 data (see Section 2.4.3 for details of this method). Figure 10 shows the plot resulting from the decomposition at the 66 cm depth. The value selected for the seasonal subset is 96 records (daily data). Panel A plots the raw temperature time series data (Y_t), panel B is the seasonal component (S_t), panel C plots the annual trend (T_t) in the data and panel D represents the random component (R_t).

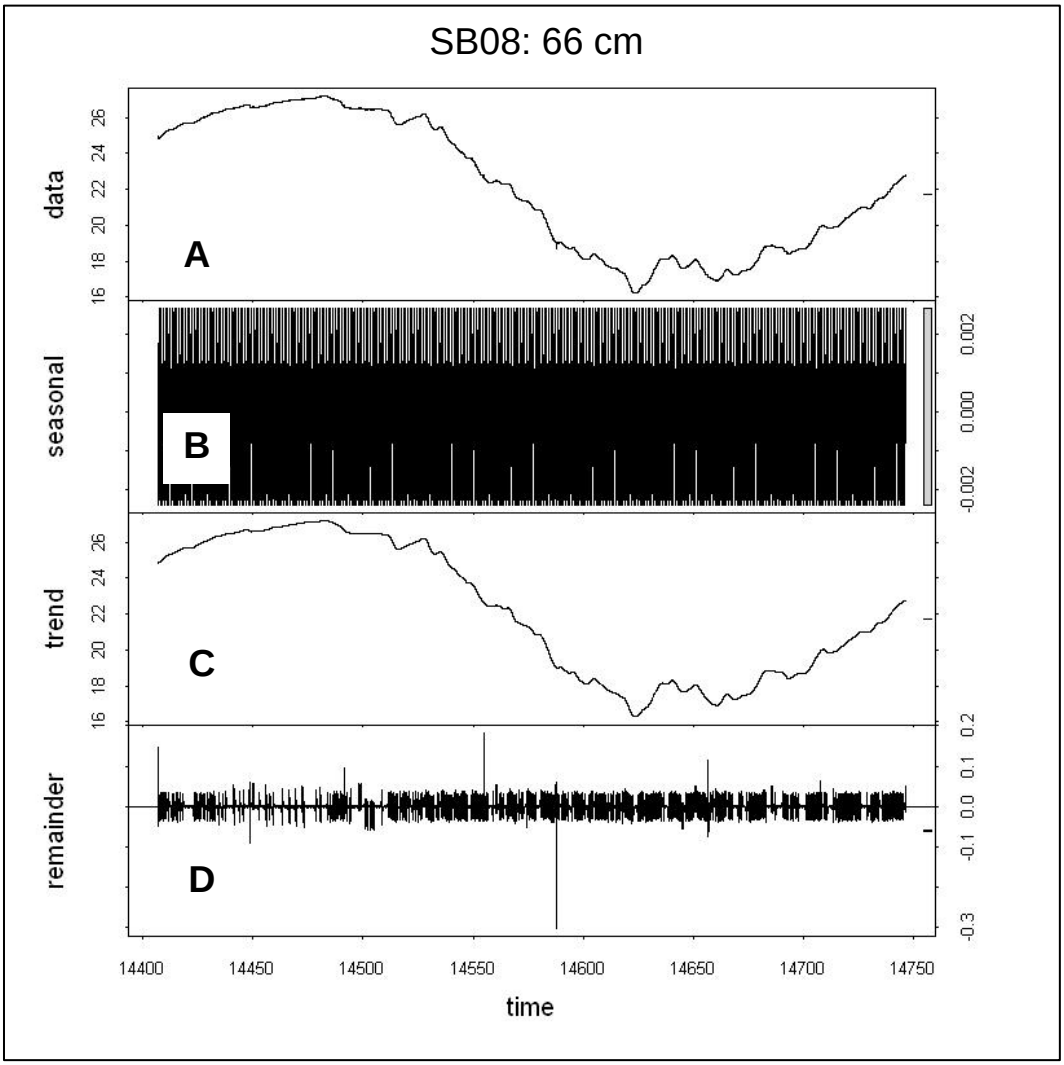

Figure 10: Decomposition of temperature of the SB08 data at 66 cm depth. Panel A is the raw data, panel B is the daily temperature oscillation, panel C is the trend over 300 days and panel D is the remainder or random component. The time displayed on the x-axis is in Julian days. R uses an arbitrary start date of January 1, 1970.

After removing the trend from the time-series, the seasonal and random oscillate around zero (Figure 10). The positive and negative values of the seasonal represent modeled

temperatures above or below the trend line while the random are the residuals of modeled and observed temperature data. Figure 11 is a conceptual diagram showing how the random component is created from the de-trended seasonal component.

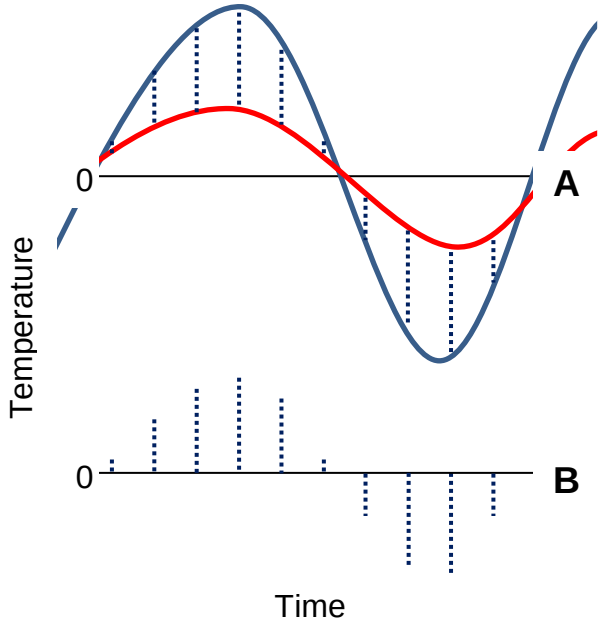

Figure 11: Conceptualized view shows generation of the random component from the de-trended seasonal component. Vertical bars in panel (A) represent the differences in temperature between modeled (red) and the de-trended observed temperature (blue). Panel (B) displays the resulting random component resulting from the differences plotted as vertical bars; positive temperature values result when the modeled data is below the observed data (positive residuals) and negative temperature values result when the observed data is below the modeled data (negative residuals).

Essentially the random component explains how well the model fit the observed data. Large values indicate a poor fit to the model and small values indicate a good fit. Outliers

occur in the random component when there are abnormal temperature changes in the observed data. Outliers caused by anomalous temperatures are indicated in Figure 10D. Similar outliers were evident at all depths also owing to abnormalities in the observed data. The overall magnitude of the random component and frequency of outlier's decreases with depth as a result of the natural attenuation of the surface signal with increasing depth as the heat capacity of the saturated sediments disperses thermal energy [*Constantz,* 2008]. This natural smoothing of the temperature profile enables more precise modeling with STL and subsequently less randomness with depth.

It is assumed that time lags between outliers at two different/consecutive depths will aid into the direct calculation of water velocity using the depth to time relationship. Figures 12 and 13 depict the random components at the 33 and 66 cm depths for the summer and winter periods respectively. Only values exceeding the sensor precision of ±0.0625 °C are deemed significant in the selection of outliers. Velocity estimates were derived using the time lag between the selected outliers at the 33cm and 66 cm depths. Summer and winter values derived from the largest outliers, were 11 and 45 mm d^{-1}, respectively (Figures 12 and 13). However, as discussed below, it was not possible to derive an average rate using all the outliers for the summer and winter periods. Velocities were converted to specific discharge and for comparison purposes are listed in Table 4.

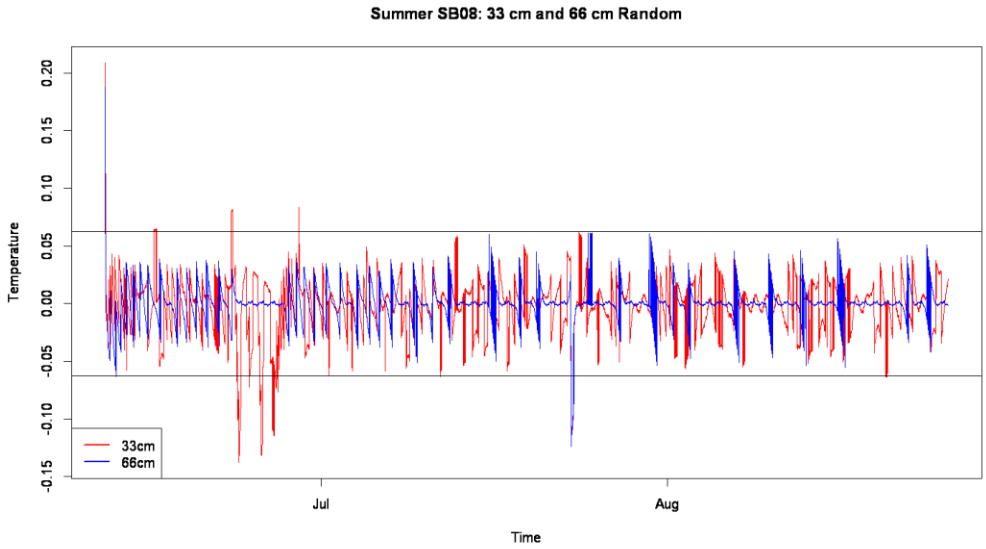

Figure 12: Random components for the 33cm (red) and 66 cm (blue) depths during summer period. Horizontal bars at ±0.0625 °C are the sensor precision. Time lag is calculated using outliers greater than sensor precision.

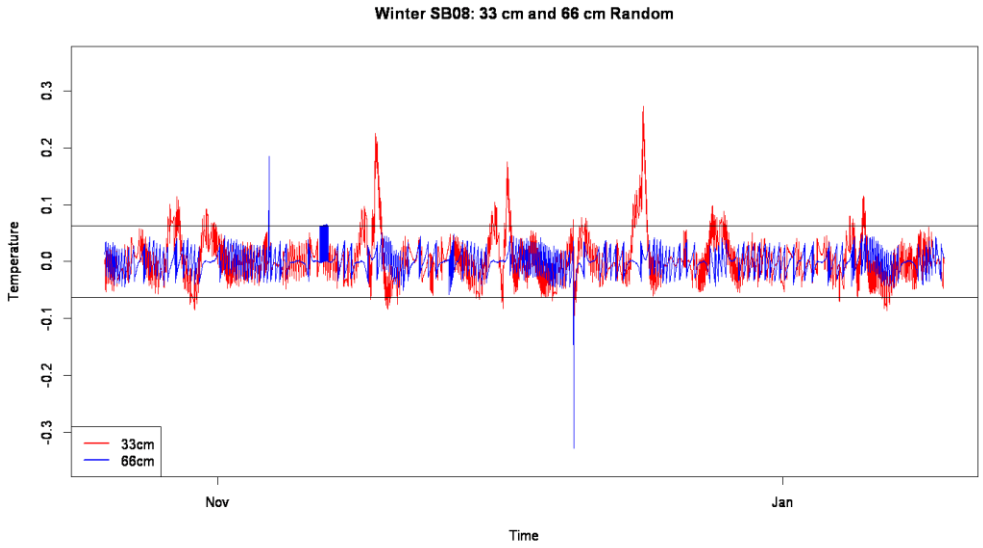

Figure 13: Random components for the 33cm (red) and 66 cm (blue) depths during winter period. Horizontal bars at ±0.0625 °C are the sensor precision. Time lag is calculated using outliers greater than sensor precision.

Table 4: Decomposition Derived Specific Discharge

Period	q (mm d^{-1})
Summer	7.0
Winter	29.0

In theory, if the modeled and observed data fit is perfect, the random component will be zero and, based on the hypothesis, this would imply that heat transfer due to advection is zero. However the lack of a random component does not guarantee that advection is nonexistent as it may be occurring simultaneously with conduction suggesting that advection and conduction can't be separated using the STL method. A visual inspection of the one-dimensional steady state advection-conduction equation (Equation 2) reveals why it may not be physically possible to separate them. When the specific discharge (q) in the second term on the left is equal to zero, changes in temperature over time are due strictly to conduction giving the impression that heat advection and conduction can be physically separated. However the conductive term on the left can only be cancelled if the thermal conductivity (K_T) is zero, which assumes that the streambed sediments are perfect insulators. This suggests that advection cannot occur without conduction and it's not possible to separate them physically thus making the hypothesis using the decomposition method irrelevant.

Assuming that it was possible to separate advection and conduction, velocity estimates from the time lag in outliers between two depths is unreliable because the overall magnitude of the random component depends on the ability of STL to model the daily temperature. Furthermore, if the subset size does not match the fundamental daily frequency of 96 records the model will not approximate the observed daily data well and will result in artificially over or under-estimating the magnitude of the random component [*Cleveland* et al., 1990] and subsequently any velocity estimates determined using the time lag and depth. As the size of the subset decreases below 96 records, the larger the random component will become and eventually the random component is transformed into an averaged representation of the raw data as the subset approaches one. This suggests that using the lag time between two outliers at different depths of the random component to derive a water velocity is equivalent to applying the time-lag method to the maximum or minimum temperatures observed in the raw data which results in a rate of heat transfer. However this rate of heat transfer between two depths does not indicate if it is owing to heat advection or conduction and thus any derived water velocities using this method are purely speculative. Support for this can also be seen when looking at the summer and winter periods (Figures 12 and 13). Prominent negative outliers appear that occur at or near the same time (i.e. t=0), if we apply the time lag method, the velocity approaches infinity as the time approaches zero. When these outliers are included in the calculation the resulting velocity is unrealistic and since there

is no basis for excluding them, it is assumed that water velocity can't be estimated using the decomposition method.

Additionally if the trend and seasonal components that created the random components in Figures 12 and 13 are added back together and plotted the resulting temperature profile should result from pure conduction if the STL method is capable of separating advection and conduction. If we plot these recomposed components against a VS2DH modeled temperature profile for the purely conductive state (q=0) then the VS2DH and the recomposed STL components should be in relatively close agreement. However, the contrary is observed for these data sets, implying that the recomposed components still contain advective information thus supporting the conclusion that it is not possible to separate advection and conduction with STL.

However there may be some utility of a random component using a method other than STL. If the random component was derived using the fit of a harmonic function to the raw data, it may represent changes in amplitude and phase shift. Hatch et al. [2006] exploited this idea as it relates to the original work by Stallman [1965]. In this work, Hatch et al. [2006] showed that groundwater fluxes could be derived by analyzing phase shift and amplitude changes between harmonic signal fit to the daily observed data of the temperature profiles of two different depths. However, since STL fits a smoothed model to the observed data it is not capable of modeling harmonic functions and would not be a

good candidate for such analysis [*Pickers* and *Manning,* 2015]. Consequently using the methods employed by Hatch et al. [2006] may be simpler and more reliable.

3.4. Geophysical Method: Electrical Resistivity

The ERT-derived resistivity ranged from 0.10–41.8 Ω m (Figures 1A and B) showing the presence of an overall less conductive media (i.e. green range) [*Samouelian* et al., 2005]. Table 5 lists the TBR derived resistivity values used to help identify the composition of zones of interest in the ERT tomographs. TBR measurements show that the bulk of the imaged surface (i.e. green range, Figure 14A and B) is equivalent to the resistivity of saturated stream sediments. ERT images show several areas near ground surface that appear to have a preferential horizontal orientation. These features could be the results of preferential horizontal groundwater flow in the clay sediments or a characteristic of the dipole-dipole array [*Samouelian* et al., 2005]. Low resistivity zones (0.375 Ω m; depicted by intermediate to dark blue colors) are likely low conductivity sediments (semipermeable) while higher resistivity (5 to 42 Ω m; yellow to red colors) zones at shallower depths (right side Figure 14A and B) are depicting more conducting sediments. The resistivity of porewater between the different zones is not expected to vary to such a degree that would result in such large differences in resistivity.

Table 5: TBR Derived Resistivities

Medium	ρ (Ω m)
Surface Water	1.77
Pore Water	0.375
Saturated Stream Sediments	2.79

Buried concrete and other construction materials were evident throughout the study site and may be the remnants of bridge construction. This may explain the large lower electrical conductivity zone (red) about 3 m below the streambed (Figures 14A and B). It was originally thought this zone might represent fresher water (less conductive); however considering the electrically conductive nature of the surface water, groundwater and the clay sediments, this is unlikely (AGI unpublished material). Since the difference-image indicates this zone is becoming less electrically conductive with time, an alternative explanation for this anomaly is possibly a leaking 10.2 cm PVC municipal water main buried below the streambed and crossing a few meters upstream from and parallel with the resistivity transect. Personal communications with the landowner confirmed the burial depth and the likelihood of water leaking as the water main is often damaged during flood events. The slow introduction of fresh water into the streambed sediments from the pipe is a plausible explanation for this anomaly.

Little differences (up to 8% changes in resistivity/conductivity) were noted between base and monitor images indicating water migration is slow [Nyquist et al., 2008]. Figure 14A (black rectangle) depicts some areas that are becoming more electrically conductive with time. Field observations during the survey identified water saturated depressions in the sediments near these locations. The increase in conductivity here may be explained by the increase in saturation of the clay-rich soils due to infiltrating surface water thus making them more electrically conductive [*Samouelian* et al., 2005]. Furthermore, evaporation likely affects the stagnant water at the ground surface, increasing salt contents, thus resulting in a more conductive infiltrating fluid [*Nyquist et al*., 2008].

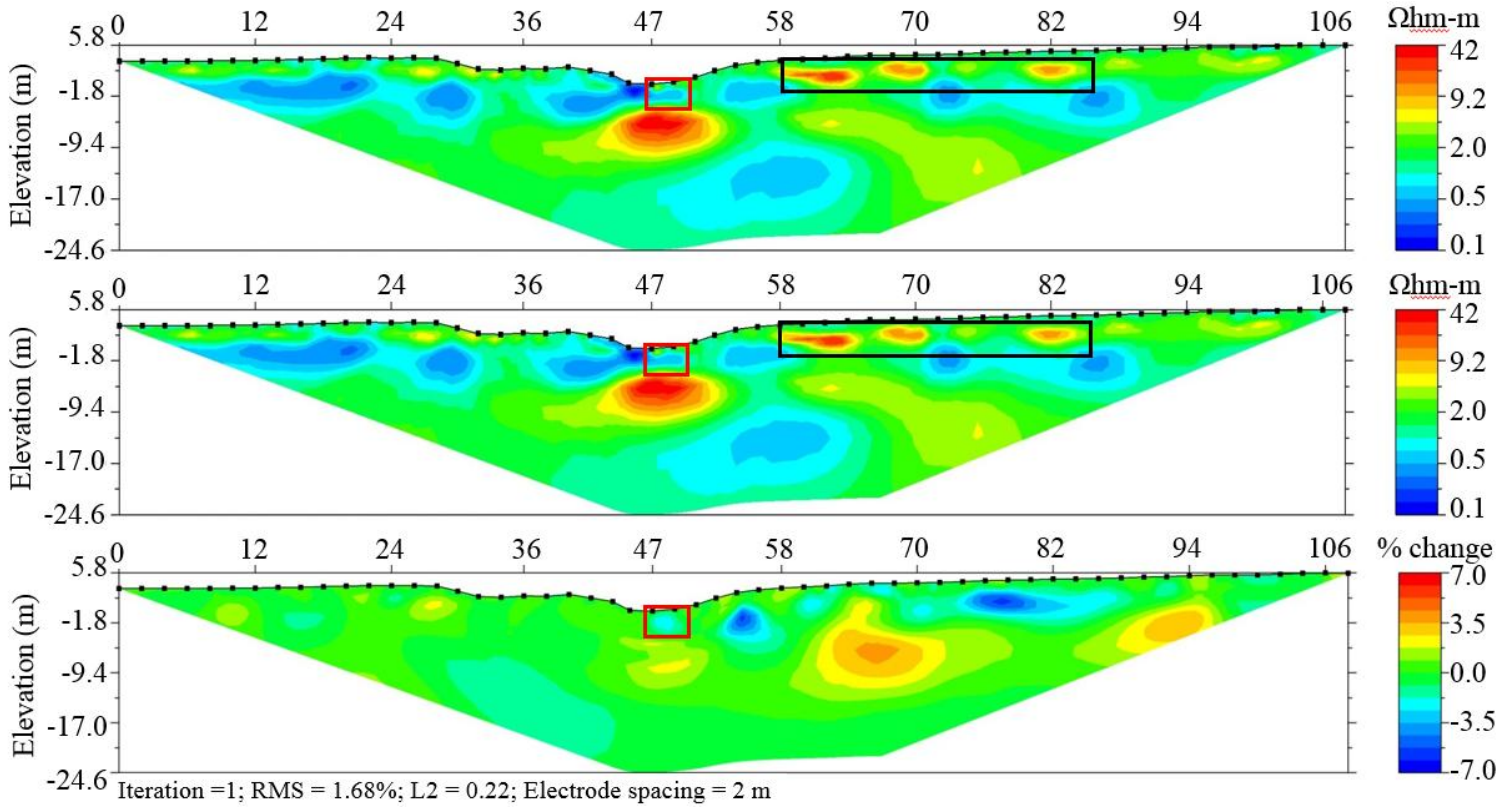

Figure 14: ERT inversion images depicting: (A) base data, is the resistivity collected at time step 0; (B) monitor data, resistivity data collected at the 3.5 h interval; (C) percent change in bulk resistivity during the 3.5 hour time-span. The red box indicates the location of groundwater discharge below the streambed. In A and B, red colors (black box) define less electrically conductive sediments while blue colors indicate sediments with greater electrical conductivity. RMS errors for the base, monitor data, and time-difference image were 9.8, 9.7, and 1.68%, respectively and corresponding L2-norm of 0.87, 0.88, and 0.22, respectively.

A groundwater flux was derived using the salt mass balance method using a 4 m^2 area, just below the stream (Figure 15). The plume selected showed a % change in bulk resistivity (up to +/-7%) exceeding the time-lapse inverted image RMS error of 1.7%. Using the percent change and the values for salinity obtained from the boxed zones in the images, (S1 and S2 were 16.7 ppt and 16.3 ppt respectively) the daily groundwater average exchange rate is 162 mm d^{-1} per 100 cm of streambed (or 16.2 mm d^{-1} per 10 cm of streambed) (Table 6).

Table 6: ERT Derived Specific Discharge

Period	q (mm d^{-1} per 0.01 m^2 of streambed)	q (mm d^{-1} per 1.0 m^2 of streambed)
Summer	16.2	162.0

It should be noted that a salt-mass balance approach does not differentiate between the vertical or horizontal input of salts in the box model. Since a horizontal conduit of water flow is visible from the ERT images, it is likely that the larger estimate includes a hyporheic component in addition to vertical upwelling. When extrapolating the thermal method-estimated fluxes to a 100 cm streambed length, assuming a 10 cm diameter of the thermal sensors, the ERT measurements are in good agreement with results of other methods. Resistivity data were collected during the summer season, outside the thermal monitoring dates. While streamflow conditions are similar and characteristic to the summer season, given the long drought record experienced by South Texas, hydrologic

conditions may have changed substantially [*USGS*, 2015]. Nevertheless, the electrical resistivity method serves as a validation tool for the estimates derived from thermal profiling, confirming the interaction between groundwater and surface water in a coastal low-flow stream.

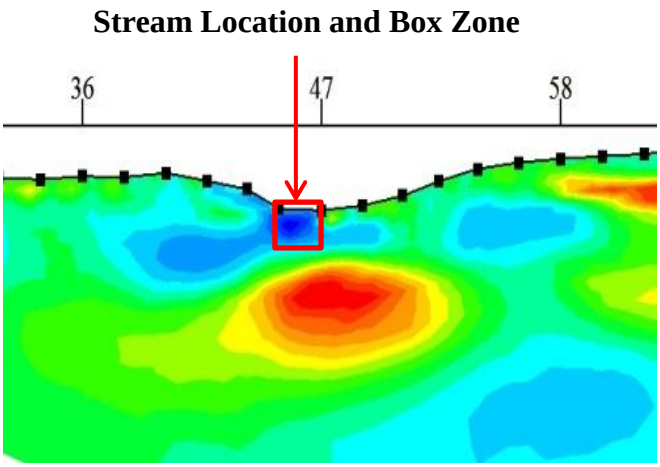

Figure 15: Zoomed in image of the base data set. The arrow indicates the stream location. The red box indicates the zone in the underlying sediments used to estimate groundwater discharge. The blue color indicates saline water below the stream based on the TBR results.

4. Conclusions

As is common with fine textured material, the conduction of heat appears to be the dominant thermal transport process occurring along the study reach in this investigation during the study period; however, it is evident that groundwater discharge to the stream is occurring to some extent for both winter and summer periods. Analysis of the data from the analytical and numerical methods suggests that during the summer period groundwater discharge to the stream was slightly higher when compared to winter. These differences may bear the result of mixing in the hyporheic zone caused by a combination of increased stream flow and stage during the winter period. Alternatively, the specific discharge resulting from the STL method indicates upwelling is greater during the winter, which is likely the result of large air temperature fluctuations that frequently occur in South Texas during the winter.

These temperature fluctuations, driven by cold fronts from the north, rapidly reduce surface temperatures and these affects usually subside after a few days when the surface temperature rebounds rapidly as the wind shifts to a more southerly direction. The resulting surface temperature fluctuations make modeling the temperature with STL more difficult, which consequently increases the magnitude and frequency of outliers in the random component during the winter. Also, as mentioned in Section 3.3, using the correlation of outliers in the random component to derive a flux is purely speculative as there is no basis for correlating the outliers since they simply represent the ability of STL to model the data. Furthermore, the underlying hypothesis that decomposition using STL

can physically separate advective from conductive heat transfer may not be possible since advection and conduction cannot be recognized uniquely [*Jobmann and Clauser*, 1994].

Resistivity-derived groundwater fluxes although considerably larger, are indicating that a horizontal flow component exists. This suggests that the vertical flow assumption of the analytical and numerical methods may be violated. Table 7 summarizes the results from all methods.

Table 7: Summary of Results from the Different Methods

Method	Summer q (mm d^{-1} per 0.01 m^2 of streambed)	Summer q (mm d^{-1} per 1 m^2 of streambed)	Winter q (mm d^{-1} per 0.01 m^2 of streambed)	Winter q (mm d^{-1} per 1 m^2 of streambed)	Flow Direction
Thermal: Numerical	11.5	115.0	4.0	40.0	Upward
Thermal: Analytical	6.7	67.0	3.0	30.0	Upward
Thermal: STL	7.0	70.0	29.0	290.0	Assumed Upward
Geophysical: ERT	16.2	162.0	N/A	N/A	Assumed Upward

Note on Table 7: For comparison purposes the analytical and numerical results between depths were averaged. The STL results are based on the largest outliers and velocities have been converted to specific discharge while the ERT-derived flux is based on the maximum percent change in porewater salinities. Since the STL and ERT methods do not indicate a flux direction, the direction is not indicated in the table although we assume upwelling is occurring based on analytical and numerical results. No ERT data was available for the winter period.

It is important to mention that uncertainty in parameters can lead to uncertainty in specific discharge. However due to the unique conditions encountered in Texas coastal streams (high percentage of water, fine-textured streambed sediments, and flat topography), most of the parameters used in this study are outside the typical ranges explored by other researchers. For example; if typical sediment values are used for thermal conductivity in the numerical and analytical thermal estimates, the resulting specific discharge is near zero. This would not be a good estimate of specific discharge since these 'typical' values do not well represent conditions at the site. Furthermore, quantitative differences between the analytical and numerical method estimates of specific discharge can be explained by how each addresses boundary conditions. The analytical method assumes boundary conditions are steady-state while the numerical solution allows for time varying boundary conditions. Consequently the analytical solution will typically overestimate specific discharge however the opposite was realized in this study. Uncertainty in the STL decomposition method depends on which outlier is used in the calculation and can result in specific discharge ranging from very small values to infinity. Uncertainty in the ERT specific discharge mainly stems from target size estimates and the RMS errors associated with the percent difference. Larger target size and larger percent difference would increase specific discharge and the converse is true for a smaller target size and percent difference.

5. Summary

The four methods examine surface water exchanges with groundwater from different approaches, and are not fully comparable in some cases. Estimates provided by the numerical and analytical solutions indicate upwelling is occurring at an average of 9 mm d-1 and 3.5 mm d-1 during the summer and winter periods respectively. STL decomposition results are more hypothetical and lack agreement with the first two methods, indicating more work needs to be done for this method to be useful; for example, this method should be applied to streambed temperature time series data for course material, where advective heat transport often dominates, and then compared with the first two methods for the same course-material data. Resistivity results provided a good first order approximation of flux considering inherent error. Thus numerical, analytical, and geophysical estimates of groundwater discharge provide good insight into streambed hydrologic processes for the study reach along this low gradient, low flow coastal stream. However, decomposition methods are not capable of separating heat advection from conduction, thus likely not serving as realistic tools for characterization of surface-groundwater water interaction for fine-textured streambeds and low gradients.

Literature Cited

Anderson, M. P. (2005), Heat as a Ground Water Tracer, *Ground Water*, 43, 951–968, doi: 10.1111/j.1745-6584.2005.00052.x.

Anibas, C., J. H. Fleckenstein, N. Volze, K. Buis, R. Verhoeven, P. Meire, and O. Batelaan, (2009), Transient or steady-state? Using vertical temperature profiles to

quantify groundwater–surface water exchange. *Hydrol. Process*., 23, 2165–2177. doi:10.1002/hyp.7289.

Bhaskar, A. S., J. W. Harvey, and E. J. Henry (2012), Resolving hyporheic and groundwater components of streambed water flux using heat as a tracer, *Water Resour. Res*., 48, W08524, doi:10.1029/2011WR011784.

Bighash, P. and D. Murgulet (2015), Application of factor analysis and electrical resistivity to understand groundwater contributions to coastal embayments in semi-arid and hypersaline coastal settings, *Science of the Total Environment*, 532, 688-701, doi: 10.1016/j.scitotenv.2015.06.077

Bredehoeft, J. D., and I. S. Papadopulos (1965), Rates of vertical groundwater movement estimated from the Earth's thermal profile, *Water Resour. Res*., 1(2), 325–328, doi:10.1029/WR001i002p00325.

Briggs, M.A., L.K. Lautz, S.F. Buckley, and J.W. Lane, (2014), Practical limitations on the use of diurnal temperature signals to quantify groundwater upwelling, *Journal of Hydrology*, 519, 1739-1751. http://dx.doi.org/10.1016/j.jhydrol.2014.09.030

Bureau of Economic Geology (1975), Corpus Christi Sheet, Geologic Atlas of Texas, Bureau of Economic Geology, University of Texas at Austin, scale 1:250,000. Available online at: http://www.twdb.state.tx.us/groundwater/aquifer/gat/

Capuano, R. M. and R. Z. Jan (1996), In Situ Hydraulic Conductivity of Clay and Silty-Clay Fluvial-Deltaic Sediments, Texas Gulf Coast, *Ground Water*, 34, 545–551. doi:10.1111/j.1745-6584.1996.tb02036.x

Carslaw, D. C. (2005) On the changing seasonal cycles and trends of ozone at Mace Head, Ireland, *Atmos. Chem. Phys*, 5, 3441-3450.

Cleveland, R.B., W.S. Cleveland, J.E. McRae and I. Terpening (1990), STL: A Seasonal-Trend Decomposition Procedure Based on Loess, *J. Official Statist*., 6, 3-73.

Constantz, J., R. Naranjo, R. Niswonger, K. Allander, B. Neilson, D. Rosenberry, D. Smith, C. Rosecrans, and D. Stonestrom (2016), Groundwater exchanges near a channelized versus unmodified stream mouth discharging to a subalpine lake, *Water Resour. Res*., 52, 2157–2177, doi:10.1002/2015WR017013.

Constantz, J., C. A. Eddy-Miller, J. D. Wheeler, and H. I. Essaid (2013), Streambed exchanges along tributary streams in humid watersheds, *Water Resour. Res*., 49, 2197–2204, doi:10.1002/wrcr.20194.

Constantz, J. (2008), Heat as a tracer to determine streambed water exchanges, *Water Resour. Res*., 44, doi:10.1029/2008WR006996.

Constantz, J., M. H. Cox, and G. W. Su (2003), Comparison of Heat and Bromide as Ground Water Tracers Near Streams, *Ground Water*, 41, 647–656, doi: 10.1111/j.1745-6584.2003.tb02403.x.

Constantz, J. and D. A. Stonestrom (2003), Heat as a tracer of water movement near streams, in *Heat as a Tool for Studying The Movement of Ground Water Near Streams*, edited by D. A. Stonestrom and J. Constantz, *U.S. Geol. Surv. Circ., 1260*, 1–6.

Constantz, J., Thomas, C.L. and Zellweger, G. (1994), Influence of Diurnal-Variations in Stream Temperature on Streamflow Loss and Groundwater Recharge. Water Resources Research, 30, 3253-3264.

Cox, M. H., G. W. Su, and J. Constantz (2007), Heat, Chloride, and Specific Conductance as Ground Water Tracers near Streams, *Ground Water*, 45, 187–195, doi: 10.1111/j.1745-6584.2006.00276.x.

Cuthbert, M. O., and R. Mackay (2013), Impacts of nonuniform flow on estimates of vertical streambed flux, *Water Resour. Res*., 49, doi:10.1029/2011WR011587.

Davis, S. N., G.M. Thompson, H.W. Bentley, and G. Stiles (1980), Ground-Water Tracers — A Short Review. *Ground Water*, 18, 14–23, doi: 10.1111/j.1745-6584.1980.tb03366.x.

Dimova, N. T., P. W. Swarzenski, H. Dulaiova, and C. R. Glenn (2012), Utilizing multichannel electrical resistivity methods to examine the dynamics of the fresh water–seawater interface in two Hawaiian groundwater systems, *J. Geophys. Res*., 117, C02012, doi:10.1029/2011JC007509.

Figura, S., D. M. Livingstone, E. Hoehn, and R. Kipfer (2011), Regime shift in groundwater temperature triggered by the Arctic Oscillation, *Geophys. Res. Lett*., 38, L23401, doi:10.1029/2011GL049749.

Freeze, R.A., and J.A. Cherry (1979), *Groundwater*: Prentice-Hall, Englewood Cliffs, N.J.

Fritz, B. G., and E. V. Arntzen, (2007), Effect of Rapidly Changing River Stage on Uranium Flux through the Hyporheic Zone. *Ground Water*, 45, 753–760. doi:10.1111/j.1745-6584.2007.00365.x.

Gealy, E.L., (2007). Saturated bulk density, grain density and porosity of sediment cores from the western equatorial Pacific, 2007-05, Deep Sea Drilling Project, 1081-1104.

Hatch, C. E., A. T. Fisher, J. S. Revenaugh, J. Constantz, and C. Ruehl (2006), Quantifying surface water–groundwater interactions using time series analysis of streambed thermal records: Method development, *Water Resour. Res.*, 42, W10410, doi:10.1029/2005WR004787.

Healy, R.W., and A.D. Ronan. (1996), Documentation of computer program VS2DH for simulation of energy transport in variably saturated porous media -- modification of the U.S. Geological Survey's computer program VS2DT. U.S. Geological Survey Water-Resources Investigations Report 96-4230, 36, Reston, Virginia: USGS.

Jensen, J. K., and P. Engesgaard. (2011), Nonuniform Groundwater Discharge across a Streambed: Heat as a Tracer, *Vadose Zone J.*, 10, 98-109. doi:10.2136/vzj2010.0005

Jiang, B., S. Liang, J. Wangand, and Z. Xiao (2010), Modeling MODIS LAI time series using three statistical methods, *Remote Sensing of Environment*, 114(7), 1432-1444.

Jobmann, M. and C. Clauser (1994), Heat advection versus conduction at the KTB: possible reasons for vertical variations in heat-flow density, *Geophysical Journal International*, 119, 44–68, doi:10.1111/j.1365-246X.1994.tb00912.x.

Koch, F. W., Voytek, E. B., Day-Lewis, F. D., Healy, R., Briggs, M. A., Lane, J. W. and Werkema, D. (2016), 1DTempPro V2: New Features for Inferring Groundwater/Surface-Water Exchange. Groundwater, 54, 434–439. doi:10.1111/gwat.12369.

Lapham, W. W. (1989), Use of temperature profiles beneath streams to determine rates of vertical ground-water flow and vertical hydraulic conductivity (No. 2337). Dept. of the Interior, US Geological Survey; USGPO; Books and Open-File Reports Section, US Geological Survey.

Lee, M.W. and T.S. Collett (2006), A Method of Shaly Sand Correction forEstimating Gas Hydrate Saturations Using Downhole Electrical Resistivity LogData, Scientific Investigations Report 2006-5121, US Geological Survey, Reston,Virginia.

Lu, N., and S. Ge (1996), Effect of Horizontal Heat and Fluid Flow on the Vertical Temperature Distribution in a Semiconfining Layer, *Water Resour. Res*., 32(5), 1449–1453, doi:10.1029/95WR03095.

Nicolau, B.A.(2001), Water Quality and Biological Characterization of Oso Creek and Oso Bay, Corpus Christi, Texas, Center for Coastal Studies, Texas A&M University Corpus Christi, 1–124.

Nishikawa, T., K.S. Paybins, J.A. Izbicki, and E.G. Reichard (1999), Numerical model of a tracer test on the Santa Clara River, Ventura County, California, *J. Ameri. Water Resour. Assoc.*, 35, 133–142. doi: 10.1111/j.1752-1688.1999.tb05458.x.

Niswonger, R.G., and Prudic, D.E., 2003, Modeling heat as a tracer to estimate streambed seepage and hydraulic conductivity, in Stonestrom, D.A., and Constantz, Jim, eds., Heat as a tool for studying the movement of groundwater near streams: U.S. Geological Survey Circular 1260, 80-89.

Nyquist, J. E., P. A. Freyer, and L. Toran, (2008), Stream bottom resistivity tomography to map ground water discharge. *Ground water*, 46(4), 561-569.

Manheim, F. T., D. E. Krantz, and J. F. Bratton, (2004), Studying ground water under Delmarva coastal bays using electrical resistivity, *Ground Water*, 42(7), 1052– 1068.

Ockerman, D.J., and C.J. Fernandez (2010), Hydrologic conditions and water quality of rainfall and storm runoff for two agricultural areas of the Oso Creek watershed, Nueces County, Texas, 2005–08, *U.S. Geol. Surv. Scien. Invest. Report 2010–5136,* 63.

Pickers, P. A.; A. C. Manning (2014), Investigating bias in the application of curve fitting programs to atmospheric time series. *Atmos. Meas. Tech,* 7(7), 7085-7136.

Rau, G. C., M. S.Andersen, and R. I.Acworth (2012), Experimental investigation of the thermal time-series method for surface water-groundwater interactions, *Water Resour. Res.*, 48, W03530, doi:10.1029/2011WR011560.

Ronan, A. D., D. E. Prudic, C. E. Thodal, and J. Constantz (1998), Field study and simulation of diurnal temperature effects on infiltration and variably saturated flow beneath an ephemeral stream, *Water Resour. Res.*, 34(9), 2137–2153, doi:10.1029/98WR01572.

Samouelian, A., I. Cousin, A. Tabbagh, A. Bruand, and G. Richard (2005), Electrical resistivity survey in soil science: A review, *Soil Tillage Res.*, 83, 173–193, doi:10.1016/j.still.2004.10.004.

Schmidt, C., B. Conant Jr., M. Bayer-Raich, and M. Schirmer (2007), Evaluation and field-scale application of an analytical method to quantify groundwater discharge using mapped streambed temperatures, *J. Hydrol*., 347, 292–307, doi:10.1016/j.jhydrol.2007.08.022.

Shamsudduha, M.; Chandler, R. E.; Taylor, R. G.; Ahmed, K. M (2009), Recent trends in groundwater levels in a highly seasonal hydrological system: the Ganges-Brahmaputra-Meghna Delta, *Hydrology & Earth System Sciences Discussions*, 6(3), 4125.

Shope, C. L., J. E.Constantz, C. A.Cooper, D. M.Reeves, G.Pohll, and W. A.McKay (2012), Influence of a large fluvial island, streambed, and stream bank on surface water-groundwater fluxes and water table dynamics, *Water Resour. Res*., 48, W06512, doi:10.1029/2011WR011564.

Stallman, R.W., (1963), Methods of collecting and interpreting ground-water data: U.S. Geological Survey Water-Supply Paper, 1544–H, 36–46.

Stallman, R. W. (1965), Steady one-dimensional fluid flow in a semi-infinite porous medium with sinusoidal surface temperature, *J. Geophys. Res*., 70(12), 2821–2827, doi:10.1029/JZ070i012p02821.

Swanson, T. E. , B. M. Cardenas (2010), Diel heat transport within the hyporheic zone of a pool-riffle-pool sequence of a losing stream and evaluation of models for fluid flux estimation using heat, *Limnology and Oceanography*, 55, doi: 10.4319/lo.2010.55.4.1741.

TCEQ (2005), Oso Creek and Oso Bay Bacteria Total Maximum Daily Load Model Final Report, Texas Commission on Environmental Quality, www.tceq.texas.gov.

USGS (2015), USGS 08211520 Oso Ck at Corpus Christi, TX, U.S. Geological Survey, http://waterdata.usgs.gov/nwis/inventory/?site_no=08211520.

Voytek, E. B., A. Drenkelfuss, F.D. Day-Lewis, R. Healy, J.W. Lane, and D. Werkema, (2014), 1DTempPro: Analyzing Temperature Profiles for Groundwater/Surface-water Exchange. *Groundwater*, 52, 298–302, doi:10.1111/gwat.12051.

Appendices:

Appendix A: Temperature Data Pre-processing.

A1. Create function to acquire data for a specific station and depth from the database

```
get.profiler <- function(station.id,end.depth) {

Query.1 <- "select station_id,enddepth,r.enddate,r.remarks,r.storet,value from a_events e,
a_results r

    where e.tag_id = r.tag_id

    and station_id like '"

 Query.2 <- station.id

 Query.3 <- "' and enddepth = "
```

```
 Query.4 <- end.depth
 Query.5 <- " order by to_date(r.enddate,'MM/DD/YYYY'),r.remarks"
 myQuery <- paste(Query.1,Query.2,Query.3,Query.4,Query.5,sep="")
 return(myQuery)
 }
```

A1.2 Execute query for specific profiler and depth (example is for SB08)

```
temp_1 <- sqlQuery(oracle,paste(get.profiler(8,1)),as.is=TRUE)
temp_0 <- sqlQuery(oracle,paste(get.profiler(8,0)),as.is=TRUE)
temp_66 <- sqlQuery(oracle,paste(get.profiler(8,.666)),as.is=TRUE)
temp_33 <- sqlQuery(oracle,paste(get.profiler(8,.333)),as.is=TRUE)
```

A1.3. Convert dates to R format dates

```
temp_1$timecode <-
strptime(paste(temp_1$ENDDATE,temp_1$REMARKS),"%m/%d/%Y %H:%M")
temp_0$timecode <-
strptime(paste(temp_0$ENDDATE,temp_0$REMARKS),"%m/%d/%Y %H:%M")
temp_33$timecode <-
strptime(paste(temp_33$ENDDATE,temp_33$REMARKS),"%m/%d/%Y %H:%M")
temp_66$timecode <-
strptime(paste(temp_66$ENDDATE,temp_66$REMARKS),"%m/%d/%Y %H:%M")
```

A1.4. Export temperatures as data files

```
export.profiler <- function(profiler){
 write.table(temp_0,file=paste(profiler,"_d00.dat",sep=""),sep="|")
 write.table(temp_33,file=paste(profiler,"_d33.dat",sep=""),sep="|")
 write.table(temp_66,file=paste(profiler,"_d66.dat",sep=""),sep="|")
```

```
  write.table(temp_1,file=paste(profiler,"_d10.dat",sep=""),sep="|")
}
```

A2. Fix time series so that it has one row for each time interval and replace missing dates with NA's. Example script is for SB08 at the 0.0 meter level

```
dir.name <- "export_data/"

file.name <- "SB08_d00.dat"
```

A2.1. Import data from pipe delimited file without row names.

```
temp <- read.table(file =
paste(dir.name,file.name,sep=""),sep="|",header=TRUE,as.is=TRUE)
```

A2.2. Fix timecode in R format date time.

```
temp$timecode <- strptime(temp$timecode,"%Y-%m-%d %H:%M:%S")
```

A2.3. create new data frame to match the ts.fix function.

```
temp.new <- subset(temp,VALUE > 0, select=c(timecode,VALUE,ENDDEPTH))
```

A2.4. Function to scroll through the timecode of temp.new and "round" minutes to the nearest 15 minute interval.

```
fix.interval <- function(temp.new) {

for (i in 1:dim(temp.new)[1]) {

  if ((temp.new$timecode[i])$min == 0 | (temp.new$timecode[i])$min == 15 |
(temp.new$timecode[i])$min == 30 | (temp.new$timecode[i])$min == 45) {

    i = i

  } else {

    if ((temp.new$timecode[i])$min > 7 & (temp.new$timecode[i])$min < 23)
round.time <- 15
```

```
    if ((temp.new$timecode[i])$min > 22 & (temp.new$timecode[i])$min < 38)
round.time <- 30

    if ((temp.new$timecode[i])$min > 37 & (temp.new$timecode[i])$min < 53)
round.time <- 45

    if ((temp.new$timecode[i])$min > 52 | (temp.new$timecode[i])$min < 8) round.time
<- 0

    temp.new$timecode[i]$min <- round.time

#     print(paste("Count =",i,"Minutes =",(temp.new$timecode[i])$min,"Rounded
to",round.time))

  }

}

 return(temp.new)

}
```

A2.5. Check temp.new timecode for correct number days, rows and intervals

```
temp.new.info <- ts.info(temp.new$timecode)
```

A2.6. Check that temp.new intervals are 15 minutes.

```
temp.new.info <- check.interval(temp.new.info,"mins",15)
```

A2.7. Create new data set in POSIXct format and no missing dates

```
new.ts <- data.frame(timecode =
make.ts(temp.new.info$start,temp.new.info$end,temp.new.info$interval,units(temp.new.i
nfo$interval)))

new.ts$timecode <- as.POSIXct(new.ts$timecode)
```

A2.8. Convert temp.new to POSIXct format.

```
temp.new$timecode <- as.POSIXct(temp.new$timecode)
```

A2.9. Merge temp.new with new.ts. into new data set temp.fix.

```
temp.fix <- merge(temp.new,new.ts,all.y=TRUE,sort=TRUE)
```

A2.10. Find NA values in temp.fix and replace with previous day value at same time using function fix.missing.

```
temp.fix$VALUE <- fix.missing(temp.fix$VALUE)
```

A2.11. Function (fix.missing) to fill in missing temperature data with the previous day's value at the same time (96 records prior).

```
fix.missing <- function(data){
   missing <- grep(TRUE,is.na(data))
   for (i in 1:length(missing)) {
     data[missing[i]] <- data[missing[i]-96]
   }
   return(data)
}
```

A3. spike removal: Sequentially scroll through weekly plots of temp.fix and look for erroneous data (outliers)

A3.1 Create a filter for the number of records averaged. Example filter is 3 days (288 records)

```
filter.size <- 288
```

A3.2. Create limit for maximum temperature change to warrant a replacement

```
limit <- 1
```

A3.3. Spike removal function.

```
spikes.out <- function(data,filter.size=8,limit=2){
   f.spike <- rep(1/filter.size,filter.size)
```

```
    data.smooth <- filter(data,f.spike)
    for (i in filter.size:(length(data)-filter.size)) {
       if (abs(data[i]-data.smooth[i]) > limit) data[i] <- data.smooth[i]
    }
    return(data)
}
```

A3.4. Execute spikes out function on temp.fix

```
test.filter <- spikes.out(temp.fix$VALUE,filter.size,limit)
```

A3.5. The amount of time in seconds to pause between plots of weekly data.

```
sleep.time <- 1
```

A3.6. Function to automatically plot weekly data at 1 second intervals

```
for (i in 1:(length(temp.fix$timecode)/96)){
x <- temp.fix$timecode[i*96*7]
my.limits <- c(x,x+604800)
plot(temp.fix$timecode,temp.fix$VALUE,type="l",lwd=2,col="grey50",xlim=my.limits,
main=paste("From",my.limits[1],"to",my.limits[2]))
lines(temp.fix$timecode,test.filter,col="coral")
Sys.sleep(sleep.time)
}
```

A3.7. Replace out of limit temperature values in temp.fix with x's

```
x <- temp.fix$timecode[(i-1)*96*7]
my.limits <- c(x,x+604800)
```

A3.8. List data and visually inspect to determine location of x values.

```
temp.fix[grep(my.limits[1],temp.fix$timecode):grep(my.limits[2],temp.fix$timecode),]
```

A3.8. Manually replace x's with NA's. In this example script, x values are located from record 3453 to 3481.

```
start <- 3453

end <- 3481

for (i in start:end){

  temp.fix$VALUE[i] <- NA

}
```

A3.9. Re-run function fix.missing to replace NA's in temp.fix with previous days values.

```
temp.fix$VALUE <- fix.missing(temp.fix$VALUE)
```

A3.10. Visually inspect plot of time versus temperature of temp.fix

```
plot(temp.fix$timecode,temp.fix$VALUE,type="l",lwd=2,col="grey25")

lines(temp.fix$timecode,test.filter,col="orange")
```

A3.11. If visual inspection looks good, replace temperature values in temp.fix with filtered data from spikes.out.

```
temp.fix$VALUE <- spikes.out(temp.fix$VALUE,filter.size,limit)
```

A3.12. Export new filtered data set (temp.fix).

```
write.table(temp.fix,file=paste("filter_",file.name,sep=""),sep="|",row.names=FALSE)
```

A4.0. Compile all temperature data for all depths into 1 data frame for each profiler.

A4.1. Import profiler data. Example script is for SB08

```
file.name <- "filter_SB08_d00.dat"
```

```
sbp.00 <- read.table(file = file.name,sep="|",header=TRUE,as.is=TRUE)

sbp.33 <- read.table(file =
paste(unlist(strsplit(file.name,"_d"))[1],"_d33.dat",sep=""),sep="|",header=TRUE,as.is=T
RUE)

sbp.66 <- read.table(file =
paste(unlist(strsplit(file.name,"_d"))[1],"_d66.dat",sep=""),sep="|",header=TRUE,as.is=T
RUE)

sbp.10 <- read.table(file =
paste(unlist(strsplit(file.name,"_d"))[1],"_d10.dat",sep=""),sep="|",header=TRUE,as.is=T
RUE)
```

A4.2 Remove duplicate rows

```
sbp.00 <- fix.dups(sbp.00)

sbp.33 <- fix.dups(sbp.33)

sbp.66 <- fix.dups(sbp.66)

sbp.10 <- fix.dups(sbp.10)
```

A4.3. Function to remove duplicate rows.

```
fix.dups <- function(df) {
  df$dup <- duplicated(df$timecode)
  df.new <- subset(df,dup==FALSE,select=c("timecode","VALUE","ENDDEPTH"))
  return (df.new)
}
```

A4.4. Fix timecode in R format date/time

```
sbp.00$timecode <- strptime(sbp.00$timecode,"%Y-%m-%d %H:%M:%S")

sbp.33$timecode <- strptime(sbp.33$timecode,"%Y-%m-%d %H:%M:%S")

sbp.66$timecode <- strptime(sbp.66$timecode,"%Y-%m-%d %H:%M:%S")
```

```
sbp.10$timecode <- strptime(sbp.10$timecode,"%Y-%m-%d %H:%M:%S")
```

A4.5. Change field names

```
names(sbp.00) <- c("timecode","VALUE.00","ENDDEPTH.00")

names(sbp.33) <- c("timecode","VALUE.33","ENDDEPTH.33")

names(sbp.66) <- c("timecode","VALUE.66","ENDDEPTH.66")

names(sbp.10) <- c("timecode","VALUE.10","ENDDEPTH.10")
```

A4.6. Change timecode to POSIXct

```
sbp.00$timecode <- as.POSIXct(sbp.00$timecode)

sbp.33$timecode <- as.POSIXct(sbp.33$timecode)

sbp.66$timecode <- as.POSIXct(sbp.66$timecode)

sbp.10$timecode <- as.POSIXct(sbp.10$timecode)
```

A4.7. Merge all depths into one data frame based on time

```
sbp.all <- merge(sbp.00,sbp.33,by="timecode",all.y=TRUE)

sbp.all <- merge(sbp.all,sbp.66,by="timecode",all.y=TRUE)

sbp.all <- merge(sbp.all,sbp.10,by="timecode",all.y=TRUE)
```

A4.8. Export data frame for each profiler with all depths

```
write.table(subset(sbp.all,!is.na(timecode),select=c("timecode","VALUE.00","VALUE.3
3","VALUE.66","VALUE.10")),file=paste(unlist(strsplit(file.name,"_d"))[1],"_all.dat",se
p=""),sep="|",row.names=FALSE)
```

A5. Visually inspect data using filtered thermal profiles and discharge.

A5.1. Import 15 minute stream discharge values from Oso Creek

```
discharge <- read.table("osodischarge.csv",sep=",",header=TRUE)
```

```
names(discharge)[3] <- c("timecode")
```

A5.2. Fix discharge timecode to match R format.

```
discharge$datetime <- strptime(discharge$timecode,format="%Y-%m-%d %H:%M:%s")
```

A5.3. Import profiler data. Example is for SB08

```
sbname <- "filter_SB08"

sball<-read.table(file = paste(sbname,"_all.dat",sep=""),sep="|",header=T)
```

A5.4. Create subset for the profiler

```
sball$dup <- duplicated(sball$timecode)

sball <- subset(sball,dup==FALSE,select=names(sball[1:5]))
```

A5.5. Fix the time format to match R.

```
sball$timecode <- strptime(sball$timecode,"%Y-%m-%d %H:%M:%S")
```

A5.6. Merge discharge measurements with temperatures

```
sball.discharge <- merge(sball,discharge,by=c("timecode"),all.x=TRUE)
```

A5.7. Check and remove duplicate rows

```
sball.discharge$dups <- duplicated(sball.discharge$timecode)

sball.discharge <- subset(sball.discharge,dups ==
FALSE,select=c("timecode","VALUE.00","VALUE.33","VALUE.66","VALUE.10","P0
0060"))
```

A5.8. Plot filtered data at all depths with discharge in stacked charts.

```
op <- par(mfrow = c(5,1), mar = c(0.5,5,0.5,2))

plot((sball.discharge$VALUE.00),type="l", col="blue",ylab="sb08.00 filter")

plot((sball.discharge$VALUE.33),type="l", col="blue",ylab="sb08.33 filter")
```

```
plot((sball.discharge$VALUE.66),type="l", col="blue",ylab="sb08.66 filter")

plot((sball.discharge$VALUE.10),type="l", col="blue",ylab="sb08.10 filter")

plot((sball.discharge$P00060),type="l",col="blue",ylab="Discharge")
```

A5.9. Plot filtered data at all depths with discharge on 1 chart.

```
plot((sball.discharge$VALUE.00),type="l", col="red",ylab="sb08 filtered temp",)

lines((sball.discharge$VALUE.33),type="l", col="yellow",)

lines((sball.discharge$VALUE.66),type="l", col="green",)

lines((sball.discharge$VALUE.10),type="l", col="orange",)

lines((sball.discharge$P00060),type="l",col="blue",ylab="Discharge")
```

A5.10. Plot specific range of filtered data at all depth with discharge on 1 chart

```
plot((sball.discharge$VALUE.00[3000:4000]),type="l",
col="blue",ylim=c(23,32),ylab="sb08 filtered temp",)

lines((sball.discharge$VALUE.33[3500:4500]),type="l", col="blue",)

lines((sball.discharge$VALUE.66[3500:4500]),type="l", col="blue",)

lines((sball.discharge$VALUE.10[3500:4500]),type="l", col="blue",)

lines((sball.discharge$P00060[3500:4500]),type="l",col="blue",ylab="Discharge")
```

A6. Create an R time-series class data set with a frequency of 1 day (96 records) for each depth of a profiler. Example is for SB08. Time code is in Julian days. R uses an arbitrary start date of January 01, 1970.

A6.1. Function to extract start and times, number of records and interval

```
ts.info <- function(v1){

   min.date <- summary.POSIXlt(v1)[1]

   max.date <- summary.POSIXlt(v1)[6]
```

```
   date.diff <- summary.POSIXlt(v1)[6]-summary.POSIXlt(v1)[1]

   ts.interval <- round(mean(diff(v1,lag = 1),na.rm=TRUE))

   ts.nrows <- length(v1)

   ts.data <-
data.frame(start=c(min.date),end=c(max.date),period.days=as.numeric(date.diff),interval
=ts.interval,records = ts.nrows)

   rownames(ts.data) <- NULL

   return ((ts.data))

}
```

A6.2. Make time series of temperature for VALUE.00

```
sball.discharge.info <- ts.info(sball.discharge$timecode)

sball.discharge.ts <-
ts(sball.discharge$VALUE.00,frequency=96,start=c(floor(as.numeric(julian(sball.dischar
ge.info$start))),96*(as.numeric(julian(sball.discharge.info$start)) %%
1),end=c(floor(as.numeric(julian(sball.discharge.info$end))),96*(as.numeric(julian(sball.
discharge.info$end))) %% 1)))
```

A6.3. Make time series of temperature for VALUE.33

sball.discharge.info <- ts.info(sball.discharge$timecode)

```
sball.discharge.ts <-
ts(sball.discharge$VALUE.33,frequency=96,start=c(floor(as.numeric(julian(sball.dischar
ge.info$start))),96*(as.numeric(julian(sball.discharge.info$start)) %%
1),end=c(floor(as.numeric(julian(sball.discharge.info$end))),96*(as.numeric(julian(sball.
discharge.info$end))) %% 1)))
```

A6.4. Make time series of temperature for VALUE.66

```
sball.discharge.info <- ts.info(sball.discharge$timecode)

sball.discharge.ts <-
ts(sball.discharge$VALUE.66,frequency=96,start=c(floor(as.numeric(julian(sball.dischar
```

ge.info$start))),96*(as.numeric(julian(sball.discharge.info$start)) %%
1),end=c(floor(as.numeric(julian(sball.discharge.info$end))),96*(as.numeric(julian(sball.
discharge.info$end))) %% 1)))

A6.5. Make time series of temperature for VALUE.10

sball.discharge.info <- ts.info(sball.discharge$timecode)

sball.discharge.ts <-
ts(sball.discharge$VALUE.10,frequency=96,start=c(floor(as.numeric(julian(sball.dischar
ge.info$start))),96*(as.numeric(julian(sball.discharge.info$start)) %%
1),end=c(floor(as.numeric(julian(sball.discharge.info$end))),96*(as.numeric(julian(sball.
discharge.info$end))) %% 1))